UNIVERSITÀ DEGLI STUDI DI PADOVA

UNIVERSITA' DEGLI STUDI DI PADOVA

Dipartimento di Ingegneria Industriale DII

Corso di Laurea Magistrale in Ingegneria dei Materiali

MSc work carried out at the Chair of Nonferrous Metallurgy - Montanuniversität Leoben

Specific heat capacity evaluation of aluminium alloy powders via Fast Scanning Calorimetry

Relatori: Prof.ssa Irene Calliari

Prof. Dipl.-Ing. Dr.mont. Stefan Pogatscher

Laureando: Nicholas Zago

Matricola: 1179203

Anno Accademico 2018/2019

Alla mia splendida famiglia.

Abstract

This thesis work aims to analyze the temperature dependent trend in the specific heat of two different aluminum alloys, AlSi10Mg and Scalmalloy®, widely used in the technique of Additive Manufacturing for the production of metal components. This production method is still the subject of a fervent process of technological development, given the wide range of materials used and the considerable advantages offered in terms of customization of the final component. Nevertheless, during this period of innovation, several issues have been found that can reduce the efficiency of the process itself

Like all the different manufacturing processes, for the Additive Manufacturing technique it is essential to carry out an accurate design phase, both in terms of operational parameters and choice of the type of substance to be used as raw material. Among the various metal alloys that can be adopted, AlSi10Mg and Scalmalloy® are among the most suitable given their mechanical and processability characteristics. However, the optimization phase must also consider other properties, as the specific heat of the metal.

For the evaluation of the specific heat trend as the temperature varies, it was necessary to use a technique of calorimetric characterization, which allows imposing on the sample thermal conditions faithful to those actually imposed by the process itself. Among the different calorimetry techniques, the Fast Differential Scanning Calorimetry (FDSC) is certainly the most compliant. Thanks to this technique, in fact, it has been possible to impose thermal conditioning rates very close to those actually used, which would not be obtainable with conventional calorimetry techniques.

This work can be considered as divided in three different parts. In the first part, an in-depth description of the AM technique was carried out, highlighting the parameters considered crucial for process optimization and focusing mainly on the specific heat of the metal.

In the second part, all the different characterization techniques used were described from a theoretical point of view, along with describing the sampling method used.

Finally, in the third and last part of this work, the various results obtained were reported and appropriate conclusions were drawn.

The entire experimental activity was carried out at the Montanuniversität Leoben - Chair of Nonferrous Metallurgy, under the supervision of Prof. Dipl.-Ing. Dr.mont. Stefan Pogatscher.

Riassunto

Questo lavoro di tesi si pone come obbiettivo di analizzare l'andamento assunto dal calore specifico di due diverse leghe di alluminio, AlSi10Mg e Scalmalloy®, largamente impiegate nella tecnica dell'Additive Manufacturing, per la produzione di componenti metallici. Tale metodo produttivo è tuttora oggetto di un fervente processo di sviluppo tecnologico, vista l'ampia gamma di materiali utilizzabili e i notevoli vantaggi offerti in termine di personalizzazione del componente finale. Ciò nonostante, nell'arco di tale periodo di innovazione, sono state comunque rintracciate diverse cause che possono ridurre l'efficienza del processo stesso.

Come i tutti i diversi processi di produzione manifatturiera, anche per la tecnica dell' Additive Manufacturing è indispensabile svolgere un'accurata fase di progettazione, sia in termine dei parametri operativi, che di scelta della tipologia di materiale da impiegare come materia prima. Tra le diverse leghe metalliche che possono essere adottate, sicuramente AlSi10Mg e Scalmalloy® risultano essere le più incoraggianti, viste le loro caratteristiche meccaniche e di processabilità. Tuttavia la fase di ottimizzazione deve comunque considerare anche altre proprietà come il calore specifico del metallo.

Per la valutazione dell'andamento del calore specifico al variare della temperatura, è stato necessario utilizzare una tecnica di caratterizzazione calorimetrica, che permetta di imporre al campione delle condizioni termiche il più fedeli possibile a quelle realmente imposte dal processo stesso. Tra le diverse tecniche calorimetriche, sicuramente la Fast Differential Scannign Calorimetry (FDSC) risulta essere quella più conforme. Grazie a tale tecnica è stato infatti possibile imporre delle velocità di condizionamento termico molto vicino a quelle realmente utilizzate, e non ottenibili con le tecniche di calorimetria convenzionali.

Tale elaborato può ritenersi suddiviso sommariamente in tre diverse parti. Nella prima parte è stata effettuata un'approfondita descrizione della tecnica AM, evidenziando i parametri ritenuti cruciali per l'ottimizzazione del processo e soffermandosi prevalentemente sul calore specifico del metallo.

Nella seconda parte invece, sono state descritte tutte le diverse tecniche di caratterizzazione utilizzate, dal punto di vista teorico di funzionamento, descrivendo anche il metodo di campionamento utilizzato.

Infine, nella terza ed ultima parte dell'elaborato sono stati riportati i diversi risultati ottenuti, traendo opportune conclusioni.

L'intera attività sperimentale è stata effettuata presso la Montanuniversität Leoben - Chair of Nonferrous Metallurgy, sotto la supervisione del Prof. Dipl.-Ing. Dr.mont. Stefan Pogatscher.

Contents

1. Introduction

The first chapter describes the Additive Manufacturing technique, defining the different types of processes in which it can be functionally divided, and underlining the crucial parameters for the overall optimisation of the technique. With regard to these parameters, attention is given to the dependence between the specific heat and the efficiency of the manufacturing process. Finally, a brief description of the evolution of thermal analysis techniques is also made, which subsequently led to the development of the Fast Differential Scanning Calorimetry.

1.1. Additive Manufacturing

Additive Manufacturing (AM), widely known as 3D printing, is a term that identifies a whole series of manufacturing techniques and technologies in which the final product is formed through a layer-by-layer deposition, without the need to melt the material into moulds or remove it from a raw shape. Thanks to the additive nature of this class of process, compared to the traditional manufacturing, typically subtractive, AM offers the capability of manufacturing objects with high degree of geometrical freedom, reducing the weight of the components and allowing high customization (Figure 1-1). Moreover, the unmelted powders at the end of the process can be recycled and reused in the future, decreasing the usage and the waste of raw material. In the last few years these advantages have caused increased popularity and a growing demand for AM in many sectors such as automotive, aerospace, marine and medical fields.

Figure 1-1: *Additive manufacturing of a Satellite Antenna Bracket*

Depending on the power source used for layer deposition and type of raw material, currently several kinds of AM processes can be used to form metal feedstock into 3D objects, and they can divide in four categories for metals, according to with the ASTM F42 Committee on Additive Manufacturing [1]:

- Powder Bed Fusion (PBF)
    - Selective Laser Melting (SLM)
    - Electron Beam Melting (EBM)
- Direct Energy Deposition (DED)
    - Laser vs. Electron beam
    - Wire fed vs. Powder fed
- Binder Jetting
    - Infiltration
    - Consolidation
- Sheet Lamination
    - Ultrasonic Additive Manufacturing (UAM)

With this manufacturing process, it is possible to employ many different materials to create a 3D-printed object, such as thermoplastics, metals, ceramics and biochemicals. Among the different AM technologies, powder bed methods are mostly used to process metallic alloys. The general process is based on the digital design of the final part by

computer-aided-design (CAD) software, on the deposition of a thin feedstock powder layer by a wiper or a roller mechanism and on a laser, or electron beam, scanning across the powder bed line by line, totally conducted within an inert controlled-atmosphere chamber. In this way, the powders are completely or partially melted into a cylindrical segment, parallel to the built direction, or melt pool perpendicularly to the built direction.

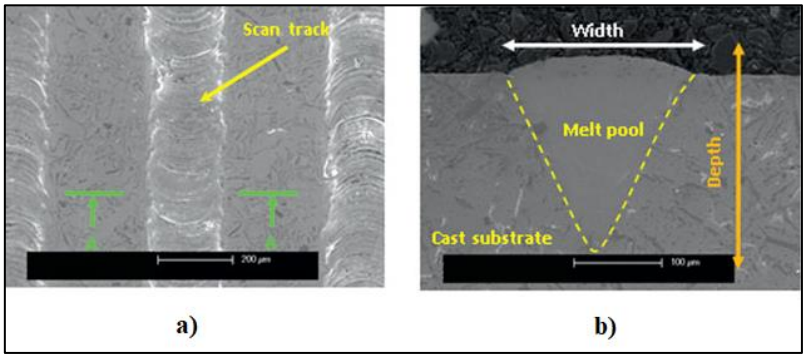

Figure 1-2: *a) Characteristic chevron pattern on top of the sample, b) cross sectional view (A-A) of a single melt pool*

The samples are formed through metallurgical bonding of scan tracks overlapping in the horizontal and vertical directions. The parts are built on a temperature-controlled build plate that acts as a heatsink (Figure 1-3), allowing the heat dissipation by lowering the thermal gradient. Thanks to this support, thermal deformations due to non-uniform thermal expansion can be avoided.

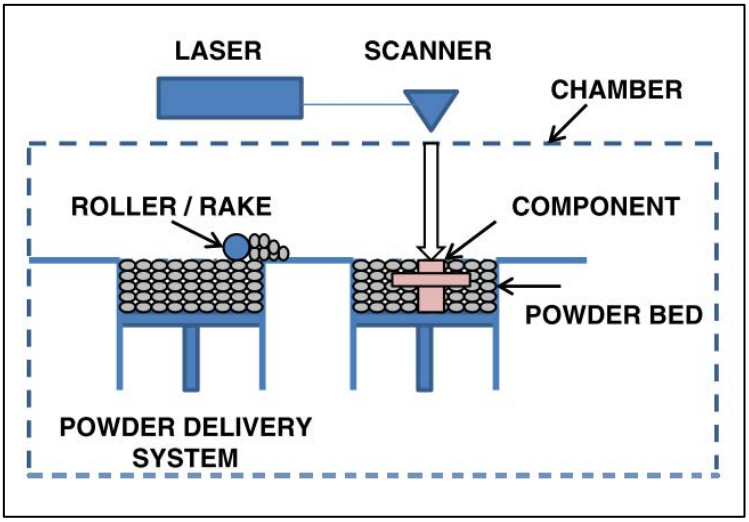

Figure 1-3 *Schematic representation of a laser powder bed fusion (LPBF)*

The advantages of design and production by additive techniques have been widely addressed recently, but it is important to underline that AM brings many interesting aspects also from a materials science perspective. This possibility is related to the high cooling rate, $10^3 – 10^6$ K/s, of the melt pool generated by successive laser scan track. The rapid cooling generates the solidification of peculiar microstructures. The fast rates of cooling, which characterize PBF processes, typically produce a fine microstructure and metastable phase, in contrast to the generally coarse microstructure developed by conventional manufacturing. For the building of the final part and the microstructure development, it needs to consider repeated material re-melting, due to the penetration of the laser beam and heat transfer. As discussed previously, the deposition process is based on the formation, track by track, of a melt pool perpendicularly of the built direction. During the scan, the laser beam is irradiated on the top surface of the powder bed. Due to this phenomenon, a series of physical and chemical processes occur in the interaction between the laser and powder materials, which include two phases: the reflectivity and the adsorption of the material's surface to the laser and heat transfer between particles, the processed part and the surrounding environment [2]. In according with Kim et al. [3], this localized material portion can be divided in three regions characterized by cells with different size and morphology: fine melt pool (FMP), coarse melt pool (CMP) and heat affected zone (HAZ).

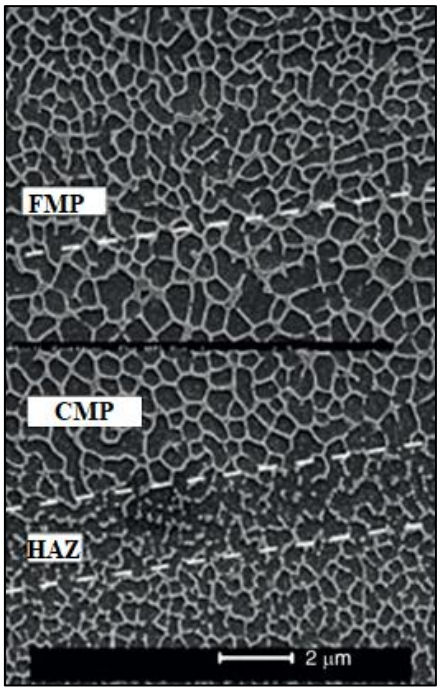

Figure 1-4: *The microstructure of AlSi10Mg created by SLM*

In the recent years AM processes found wide use in producing objects with different types of alloys, such as titanium, nickel, steels, refractory materials and aluminium. In the case of titanium alloys, employing additive techniques overcomes the problems of poor machinability and the issues related to their formability. Aluminium alloys are characterized by low density, high strength, adequate hardenability and excellent weldability. In any case, because of high solidification rate of AM, which are significantly higher compared to conventional casting process, the layer by deposition can be compared and modelled as a series of welding processes. It is not surprising that the range of printable metals alloys is limited to those known to be easily weldable. According to Martin et al. [4], during the solidification of unweldable alloys, the primary equilibrium phase solidifies first, with a different composition from the bulk liquid. This results in an enrichment of solute in the liquid near the solidifying interface, modifying the equilibrium liquidus temperature and producing an unstable, undercooling condition. As a result, a breakdown of the solid-liquid interface occurs that leads to dendritic grain growth with long channel of interdentritic liquid. As the temperature and liquid ratio decreases, volumetric solidification shrinkage due to the thermal contraction in the channel produces cavities and cracks, which can span the entire length of the columnar grain and propagate through additional intergranular regions, as shown in Figure 1-5. In contrast, fine

equiaxed grains more easily accommodate the strain in the semi-solid state by suppressing the coherency which locks the orientation of these solid dendrites and promotes tearing.

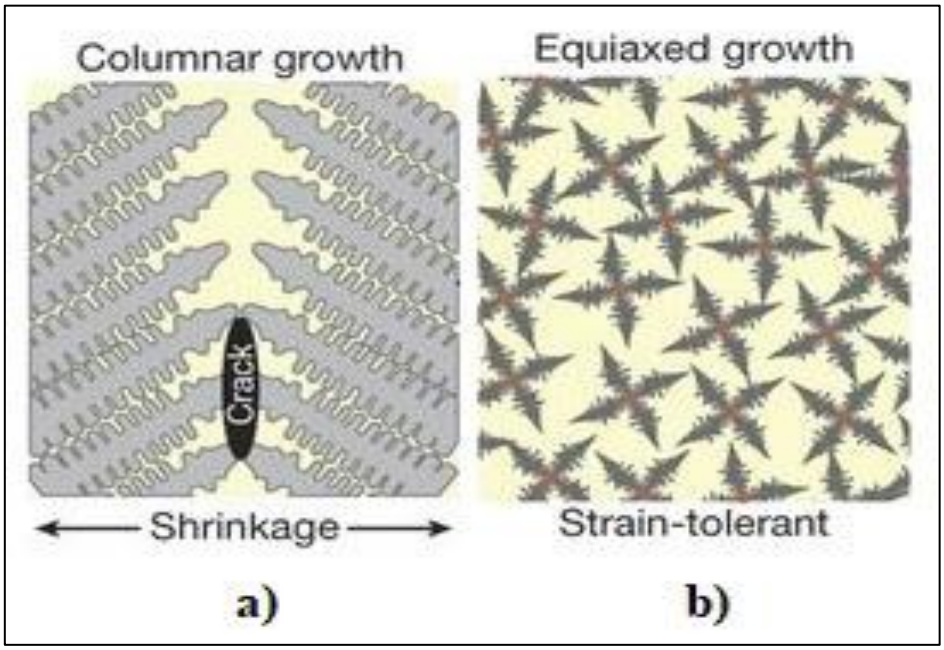

Figure 1-5: *a) columnar growth of dendrites, b) equiaxed grain growth*

Although aluminium alloys present optimal characteristics, including good weldability, which make them suitable for conventional manufacturing, the number of these alloys applied for AM is still very limited and the resultant properties are often mediocre [5,6]. Compared to other PBF candidate materials, aluminium alloys are challenging to process with additive methods. One of the main issues is related to the difficulties in spreading the powder bed due to the poor flowability of the powders. Furthermore, aluminium powder is very susceptible to oxidation that causes the formation of thin layers of oxide on the gas atomized particle surface and on the solidified materials. This characteristic can reduce the wettability and hinder the remelting of the previous layer, promoting porosity and cracking in the built parts [7,8]. Finally, fusion of aluminium alloy powders usually requires higher laser power due to their high reflectivity and the high thermal conductivity of the solidified material [9].

In the last decade, many studies have been carried out to develop improvements in aluminium alloy component production by Additive Manufacturing techniques. First, the choice of a suitable alloy, with a specific composition, was one of the main points of

interest. It has been observed that among the different Al alloys, those with mainly near-eutectic composition Al-Si alloys allow for the achievement of adequate final components [10]. Following, the studies related to AM have addressed the enhancement of the different alloys, through the addition of appropriate elements. This method avoids or reduces the formation of large columnar grains and periodic cracking [10]. A higher strengthening effect of Al alloys has been observed by alloying of specific elements to the base metal. Among all the alloying elements, the transition metal element scandium can markedly improve the alloy mechanical properties, even with only small additions [11]. Parallelly Martin et al. [4] demonstrate that this issue can be resolved by introducing nanoparticles of nucleants, previously activated, that control the solidification process during additive manufacturing (Figure 1-6).

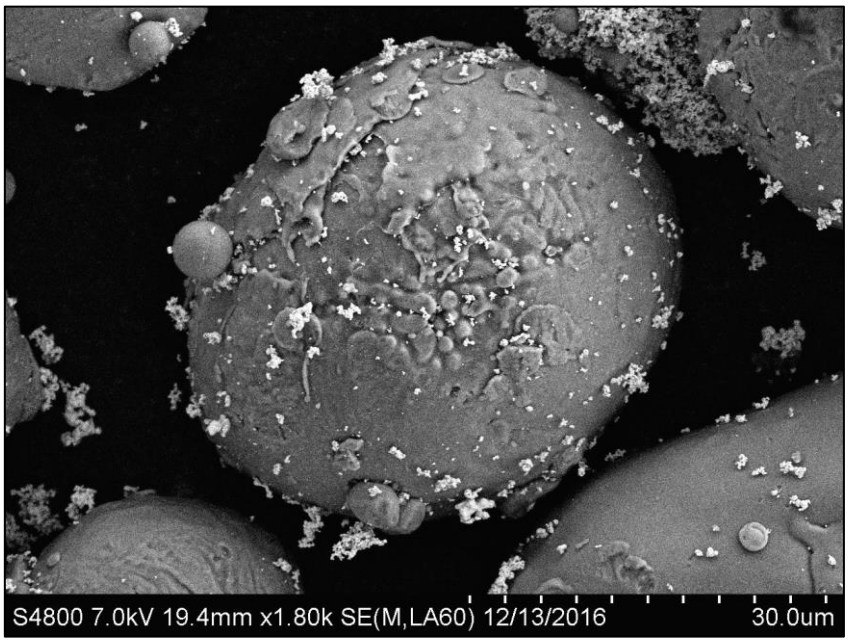

Figure 1-6: *AlSi10Mg powder with WC nanoparticles*

Further significant improvement can surely be based on an efficient optimization of the process parameters. The set of optimized parameters varies according to the type of working materials and PBF machine. The most frequently analysed parameters are processing environment, powder properties, layer thickness, laser power, scan speed, hatch spacing and scan strategy.

Generally, the PBF process is conducted in an inert atmosphere, typically argon. It is demonstrated that, in function of gas type and flow rate within the AM chamber, material densification and deposition may be subjected to variation [12,13]. For the successive deposition of uniform powder layers, the particles need to satisfy some prerequisites such as low porosity, spherical morphology, good flowability, minimal gas pores and Gaussian powder-size distribution, all of which depend on their manufactured method. Flowability is improved for spherical particles and a uniform Gaussian size distribution, while the presence of gas phase in the initial powder suppresses densification. A presinter scan strategy which involves scanning each layer twice, on the first scan with lower power than the second one, can be used as a significant remedy for a powder that does not fully comply to some of the requirements [14]. Through the examination of continuous single track and the melt pool shape, it is possible to determine the suitable laser power and scan speed for low porosity manufacture and to define the layer thickness and hatch spacing. The melt pool's stability is controlled by the process parameters: the width and the depth of scan track are related to laser power and scan speed, whereas its size is governed by the laser power and absorptivity of the material.

Current LPB machines tend to have a small laser spot size, for improving the resolution and surface finish, and high power to increase build speed. The laser or electron beam, with a defined power and scan speed, interact with a layer of powder, which is heated when it absorbs an adequate portion of laser power. If enough power is absorbed, the powder melts forming the melt pool that extends to the solid material beneath the powder and welds the new layer to the pre-existing one. In this mode, the depth of the melt pool is controlled by the thermal conduction in the material. Although for specific combinations of laser power, scan speed and beam size it is possible to modify the fusion mode, from conduction mode to so-called "keyhole mode" [15]. In "keyhole-mode", the laser power density is enough to cause the evaporation of the metal and form a plasma. Due to the evaporation, a vapour cavity is developed, and it causes an enhancement of laser adsorption. This mechanism enables the laser beam to penetrate further with respect to conduction mode. The cavity collapse can leave voids in the wake of the laser beam. The mode of melting depends on the balance between conductivity and reflectivity of the powders that defines the energy transfer efficiency during irradiation of the material with the beam. The energy transfer efficiency is defined by the ratio of energy absorbed by the material to the power used. Conduction mode occurs when this ratio is equal to the material absorptivity, whereas if the ratio is larger than the absorptivity, due to the high

reflectivity in the melt pool, the “keyhole mode” takes place. The shape of melt pool, whether spherical or conical, is an important factor in optimizing the process parameters (Figure 1-6).

The purpose is to guarantee an optimal overlap of the different melt pools to create metallurgical bonding of adjacent scan tracks in order to obtain consolidated layers, without defects. In the case of Aluminium, a conical shape has been observed and for this, a narrow hatch spacing is required. It is necessary to underline that the use of narrow hatch spacing causes a lowering of production rate, whereas the use of larger hatch spacing imposes a limitation on the maximum layer thickness [16]. Increasing the layer thickness promotes the formation of defects in the tracks and layers, hindering the deposition of uniform layers.

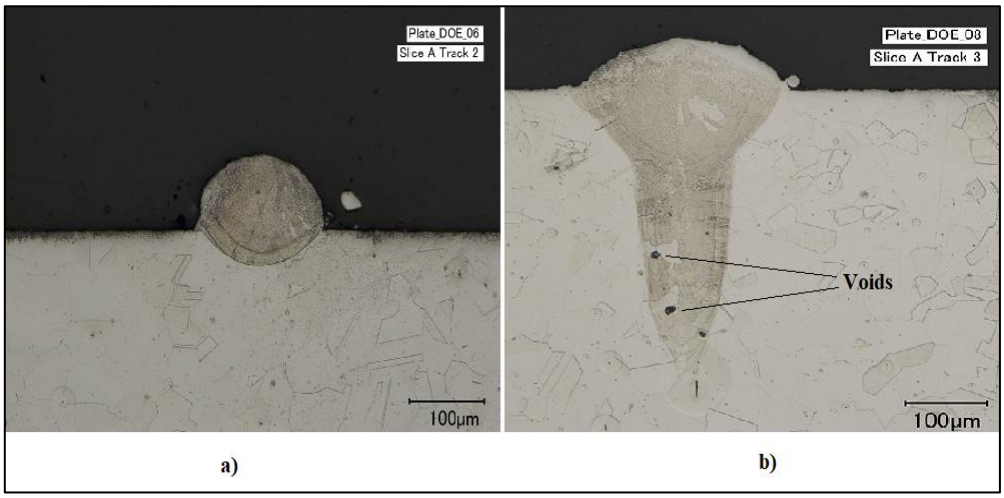

Figure 1-7: *Metallographic cross section obtained in Conduction mode (a) and Keyhole mode (b)*

Depending on the scan speed used in the AM process, two different types of porosity shape can be observed: metallurgical pores (spherical) and “keyhole” pores (irregular). It is possible to define a critical scan speed that determines which of the two pore typologies is formed [17]. For greater values than this critical speed, the formation of metallurgical pores is witnessed due to lower power supplied per unit of irradiated volume of powder. In contrast, the use of lower scan speed value causes the formation of “keyhole” pores because of the greater power provided causing the evaporation of the material. In power bed fusion processes it is possible to analyse the transition from conductivity mode to

"keyhole mode" as governed by the energy density. For this purpose, it is necessary to evaluate the different combinations of process parameters, such as power, scan speed and beam size. The identification of the specific combinations of parameters, which make it possible to define this transition, is founded on the analyses of normalized enthalpy related to the process parameter and the material. In according to King et al. [18], the threshold for keyhole mode melting can be estimated with:

$$\frac{\Delta H}{h_s} > \frac{\pi T_b}{T_m} \approx 6 \quad (1.1)$$

Where ΔH is the specific enthalpy (it defines the process attribute), T_b is the materials boiling temperature, T_m is the material melting temperature and h_s is the enthalpy of melting. The use of normalized enthalpy to combine the effects of power, speed and beam size has been experimentally validated, though it has been observed that the relation is only useful up to the threshold of "keyhole mode", whereas, beyond this limit, it does not include additional physics that exists in the keyhole formation.

During the PBF process, material properties of the alloys in the powder, molten and solid-state condition play an important role on the additive manufacturing process related to the methods of heat transfer following the melting of the different portions of materials. The cooling process of the built part, that controls its microstructure and the final properties, is determined by the rate of heat removal from the solid surface of the build. This heat transfer takes place in different locations and in different ways. On the melt front, localized at the top of the building part, the heat is lost by direct radiation to the process chamber, whereas on the orthogonal and parallel build direction, the heat is transferred by conduction and radiation to adjacent material. Thus, thermal property data such as heat capacity, thermal conductivity and surface emissivity are fundamental for the modelling of temperature evolution in 3D printing.

Among the different thermal properties considered above, an accurate assessment of the specific heat capacity of the material under processing is essential for a successful modelling procedure and therefore for producing products with optimal characteristics. For example, in relation to that previously discussed, depending on the combination of process parameters used, the melting process may occur by conduction or evaporation of the metal, with likely formation of porosity characteristics in the final solid phase. For the evaluation of keyhole threshold, the combination of the fundamental parameters can be

estimated in terms of normalized enthalpy. From Eq. (1.6), the normalized enthalpy is dependent on the value of enthalpy of melting, which is related to the specific heat capacity according to:

$$h_s = \rho c_\rho T_m \quad (1.2)$$

In which ρ is the density and c_ρ is the specific heat capacity of the powder.

In addition, it must be underlined that the value of the specific heat capacity is also strongly relevant in the evaluation of heat transfer. Considering a non-steady state condition, the thermal transfer generated between two parts placed side by side, at different temperature, is regulated by the thermal diffusivity a:

$$a = \frac{\lambda}{\rho \cdot c_\rho} \quad (1.3)$$

In which λ is the thermal conductivity of the material.

The specific heat capacity, or simply specific heat of a substance, is defined as:

> *"The heat capacity of a sample of the substance divided by the mass of the sample, or the amount of energy, in form of heat, that must be added to one unit of mass of the substance, in order to increase its temperature of one unit"*

Over the years many studies have been conducted on different metal alloys to obtain an accurate evaluation of the specific heat capacity. It is observed that from these parameters it is possible to determine not only the thermal behaviour of the analysed material but also the microstructural evolution. It is necessary to underline how the specific heat is a quantity strongly dependent on the composition of the alloy and on the temperature to which it is subjected. It has been demonstrated that the specific heat undergoes quantitative variations as a function of the percentage of alloying elements present within the alloy. This behaviour can be described through a linear relation, called Neumann-Kopp's rule [19]:

$$c_p = \sum_{i=1}^{N} (c_{p,i} \cdot f_i) \quad (1.4)$$

where N is the total number of alloy constituents, $c_{p,i}$ and f_i represent the specific heat capacity and the mass fraction of the i-th constituent. Regarding the influence of temperature, from the electron theory of specific heat, it has been concluded that the evolution of heat capacity is linear in small temperature ranges but follows power and exponential functions over larger ranges of temperature [20].

Among the different metal alloys, aluminium alloys are a class of metal materials that, for their light weight and high temperature withstandability, are widely used in industrial and technological field. The increasing usefulness of these alloys has led the researchers to want to better understand their physical properties and develop new compositions. For these reasons, a considerable amount of experimental work has been done on the heat capacity behaviour of Al alloys, at high as well as at low temperature. Hirata et al. [21], for example, studied the effect of plastic deformation after precipitation quenching in an Al-Mg-Si alloy, by hardness and specific heat measurements. Krylovisky et al. [22] measured the specific heats of pure aluminium and an aluminium-silicon alloy, from 10 - 270 K. They demonstrated that the specific heats of both are identical at temperature below 50 K, but that of the alloy increases at a slower rate than pure Al and at 270 K the specific heat capacity of the alloy is smaller. Zahra et al. [19] measured the heat capacities of different Al alloys, between 20 and 520 °C, to predict the different precipitation of metastable phases during the thermal treatment, and for several compositions.

1.2. Chip Calorimetry

As discussed extensively above, determined aluminium alloys, with specific characteristics in terms of composition and under appropriate conditions, are optimal materials to produce components by additive technologies. The optimisation of process parameters can be carried out through the analysis of the material specific heat capacity. It is easy to deduce how an accurate evaluation of the specific heat of a given Al alloy, can be performed using analysis techniques enable to simulate, as realistically as possible, the PBF process conditions. In this context, the temperature and composition dependence on the value of the specific heat must not be overlooked.

The science of calorimetry is more than 200 years old. During this time many calorimetric instruments have been devised and refined. The last two decades have witnessed a significant increase in the demand for thermal analysis and calorimetry equipment, given the strong orientation of materials science toward the analysis of thermal properties, with interest in the study of rapid phase transitions. For this new interest, a rapid development of nanocalorimetry has been necessary.

Rapid phase transitions are essential aspects in the development of materials, because the development of extreme non-equilibrium conditions can lead to the formation of metastable phases and micro-structural modification. The quantification of this phenomena is still difficult using conventional thermal analysis techniques, such as Differential Scanning Calorimetry (DSC) and Differential Thermal Analysis (DTA), because of their limited scanning rate and sensitivity. These methods allow quasi-isothermal measurements and maximum scanning rates up to 10 K/s, not enough to study rapid phase transitions. Additionally, due to the large addenda of the system, samples with masses in the order of milligrams are preferred to provide a high signal-to-noise ratio. Consequently, conventional methods cannot be used for phase transitions in a sample with low mass. Through the work conducted by Hellman et al. [23], it has been possible to reduce the addenda capacity of the system by the fabrication of thin-film calorimetry chips, with an addenda in the order of 10^{-6} J/K. This allowed heat capacity measurements of sample with a mass of only several micrograms. Several studies have been carried out in order to increase the heating rate of the sample under analysis. Hager [24] developed quasi-adiabatic calorimetry at high heating rates, ca. 500 K/s, whereas Allen and co-workers [25] designed an Electrical Thermal Annealing (ETA) capable of

ultrahigh scanning rates up to 10^6 K/s. The ETA sensor developed by Allen enabled the determination of phase transition temperatures, but it did not allow measurements of other important thermophysical properties, including the specific heat capacity. Based on the thin-film chip technology, Lai et al. [26] were able to determine the heat capacity and melting enthalpy of Sn films, heating the sample with a rate of 30,000 K/s in a vacuum chamber, with a base pressure (2.7×10^{-5} Pa). To test even thinner samples, the authors developed a direct differential technique to maximize the signal-to-noise ratio [27].

The ETA sensor was a pioneering device that served for the development of many subsequent nanocalorimeter devices, although several challenges remain unresolved. Firstly, silicon heaters act like thermistors and, by applying a high-power electrical current, the samples could be heated up to 10^6 K/s. With this configuration, a direct current impulse is necessary to measure the sample temperature. However, this applied current reduces the cooling rate, especially near room temperature. Second, the vacuum conditions reduce heat loss, but also strongly limit the maximum cooling (only a few thousand K/s). Furthermore, with this sensor it is difficult to make measurements at low heating rate, because of the non-negligible heat losses and the reduced signal-to-noise ratios. Finally, although calorimetry can obtain information concerning phase transformation energetics, it cannot reveal structural information. This issue can be solved through the coupling with another characterization technique.

While the higher heating rate can be achieved by applying higher heating power and using a smaller sample, to increase the cooling rate an enhancement of the heat loss is necessary which can be accomplished by reducing sample size. In this case, it is better to use a measurement environment filled with inert gas, for its higher thermal conductivity and low heat capacity. Additionally, to improve the cooling ability of the technique it is necessary to avoid the application of current upon the quenching. This improvement can be obtained by physical separation of the heater from the thermometer. Through implementation of all these different improvements, a single sensor non-adiabatic fast scanning calorimeter was developed, with two heaters differentially coupled. With this, it must be considered that, although conducting measurements in a gas environment increases the maximum cooling rate, the analysis of heat loss and heat capacity becomes more complex.

Further development of this technology was made possible by Rodriguez-Viejo et al. [28], who developed a digital proportional integral differential (PID) controller to maintain a better sample temperature control, particularly in the transition regions. This implementation was applied to Allen's sensors, but it was not the only change made by Rodriguez-Viejo et al. In the original work of Allen, two heaters were included in one sensor, while the new nanocalorimetric system consisted of two sensors working in parallel: one sensor was loaded the sample and the other sensor performs the function of empty reference (twin calorimeters). The presence of an empty reference reduces the influence of heat loss and addenda heat capacity on the obtained data. Finally, to improve the signal-to-noise ratio and the resolution of the device, Shick's group [29, 30] developed a power-compensated differential scanning calorimetry technique (DFSC) with two parallel sensors.

The introduction of chip-based calorimeters has led to a considerable breakthrough in the techniques of thermal analysis. Through this method, it has been possible to analyse phenomena characterized by high kinetics such as crystallization, phase transition and melting behaviour of materials. The first instrument to be commercially available was Flash DSC 1 (Metter Toledo) which aroused great interest because it allows a wide range of heating and cooling rates to be investigated: from 0,1 to 40,000 K/s. Nowadays it is widely used in several fields of material science. For example, Pogatscher et al. [31] employed this system to investigate the crystallization and phase transition behaviour of the amorphous metallic alloy $Au_{70}Cu_{5,5}Ag_{7,5}Si_{17}$ or Spieckermann at al. [32] who determined the fragility of two metallic glasses through the FDSC method. Furthermore, there is a lot of interest in this technology also in other fields such as pharmaceutical [33] and food industries.

Among the different analyses carried out using nanocalorimetry, the possibility to study the specific heat capacity, in such conditions as to allow realistic simulation of the additive process (high scanning rate processes in controlled environments), is crucial.

2. Characterization Methodology

The second chapter describes the different characterization techniques used for the development of this project. Great importance is given to the description of the techniques of thermal analysis, conventional DSC and FDSC, which are fundamental for the surveys. Regarding FDSC analyses, the different correction procedures for the analysis of experimental data are described. Finally, the operating principle and the analytical capabilities of the scanning electron microscope are also briefly described.

2.1. Calorimetric techniques

The objective of calorimetry is to measure the heat exchange that occurs in a body, appropriately conditioned at a given temperature program, when specific chemical-physical processes arise, such as melting, crystallization, phase transitions and chemical reactions. The measurements of the heat flow, released o acquired, is evaluated through the change in temperature of the body itself. Thanks to the different techniques of thermal analysis that currently exist, it is possible to measure a wide range of fundamental properties for the study of different classes of materials, e.g. mass, volume, evolved gas, thermal conductivity and specific heat capacity. The choice of the appropriate thermal analysis and temperature program to use depends on the property of interest.

Generally, two different traditional techniques can be employed for the evaluation of the thermal properties. These methods are very similar in terms of operational procedures, even though their outputs are difference.

- Differential Thermal Analysis (DTA): the signal produced represents the temperature difference between the sample and an inert reference, generally plotted versus the temperature. The DTA technique reveals changes during the sample heating, which represent phenomena of emissions or absorptions of energy. The area of an exothermic or endothermic peak is a function of the enthalpy change associated with the process.

- Differential Scanning Calorimetry (DSC): in addition to allowing the measurements of the temperature of the sample under examination, thanks to its design characteristics, this technique also allows the measurement of the sample heat flow. It is also possible to measure the heat energy (e.g. heat of melting) that is absorbed or released by the sample. With the correct experimental procedures, measurements of specific heat capacity are also possible [34].

2.1.1. Differential Scanning Calorimetry (DSC)

A "differential method of measurement" is defined as:

"a method of measurement in which the measured quantity (the measurand) is compared with a quantity of the same kind, of known value only slightly different from the value of the measurand, and in which the difference between the two values is measured [35]".

Depending on the design and measuring principle, the Differential Scanning Calorimeters must be distinguished in two basic types:

- The power compensation DSC
- The heat flux DSC

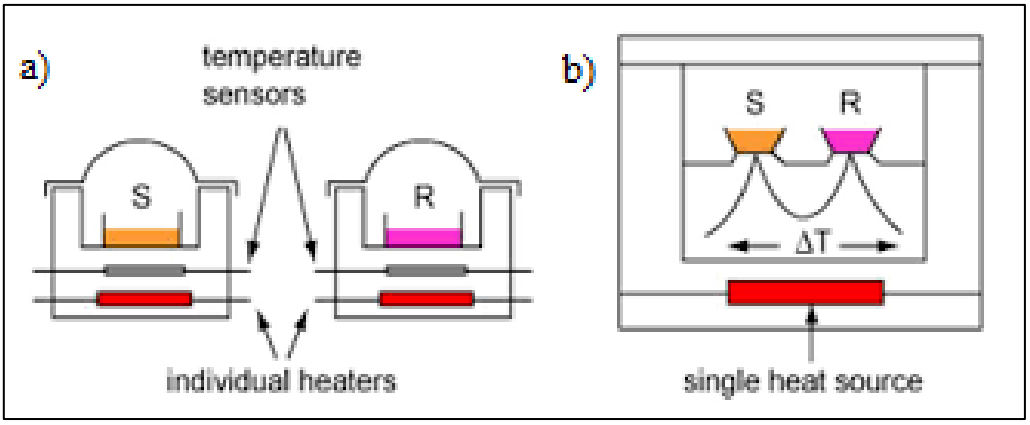

Figure 2-1: *a) Power compensation DSC b) Heat flux DSC*

In commercial power compensation DSCs (Figure 2-1 a), the measurement system consists of two identical micro-furnaces, generally produced in Platinum-Iridium alloys, both placed on an Aluminium thermostat block. In the two furnaces, the sample to be

analyzed and the reference are inserted separately in two crucibles. Each of the two furnaces also has a temperature sensor, usually in Platinum, and a heating resistor. During the imposed thermal conditioning program, the same heating power is applied to both the furnaces, via a control circuit, in order to change the temperature of the two samples. In the case of an ideal thermal symmetry, the temperature of both furnaces is always the same. When asymmetry is recorded, for example due to a phase transition in the sample, a temperature difference is observed between the two chambers. A second circuit compensates for this temperature variation by applying an increase or decrease in the thermal power to the sample. The resulting power difference is proportional to the heat flow.

In DSC instruments with heat flux mode (Figure 2-1 b), thermal analysis is always carried out using two different crucibles, one for the sample and one for the reference substance (it should be underlined that, depending on the type of analysis, the reference crucible can be left empty or not). However, unlike what has been described for the compensation mode, in this case the two crucibles are placed inside the same furnace, where they are conditioned to the same temperature program. If a change in property occurs, it is possible to measure a difference in temperature. This difference is given as a voltage in the original signal, then automatically converted into a heat flow rate ($d\Delta q/dt$) [36].

A Netzsch DSC204 F1 Phönix, shown in Figure 2-2, was used to carry out part of the thermal analyses necessary for this project.

Figure 2-2: *The Netzsch DSC204 F1 Phönix*

This instrument is equipped with a silver furnace with an embedded heating coil. The high thermal diffusivity of the silver provides an excellent heat distribution inside the cell. This characteristic is very important for the device, which works according to the heat flux principle. The possible heating and cooling rates of Netzsch DSC204 F1 Phönix are in the range 0.001 to 200 K/min, and the maximum cooling rate achievable depends on which cooling option is used, among compressed air, intracooler and liquid nitrogen. The atmosphere in the chamber should be oxidizing or inert and can be switched from one gas to another during the experiment. In any case, the presence of a protective gas does not guarantee absolute protection against oxidation phenomena at high temperatures. Different kinds of crucibles can be used in thermal analysis. In choosing the most suitable crucible, it is necessary to avoid chemical interactions with the sample and to assure its resistance in the test conditions. Generally, they are made in metal, graphite, glass or ceramic oxide.

For both operating modes, depending on the thermal properties and the characteristics of the sample to be analyzed, it is essential to implement a suitable time-temperature program to condition the specimen and the reference. In general, the thermal program is composed of a temporal sequence of segments, which define the different steps to which the sample is to be subjected. In the simplest form, these trends are composed of constant heating/cooling rate ($dT/dt \neq 0$) and isothermal segments ($dT/dt = 0$). In Figure 2-3 it is possible to observe a standard DSC program for the analysis of melting.

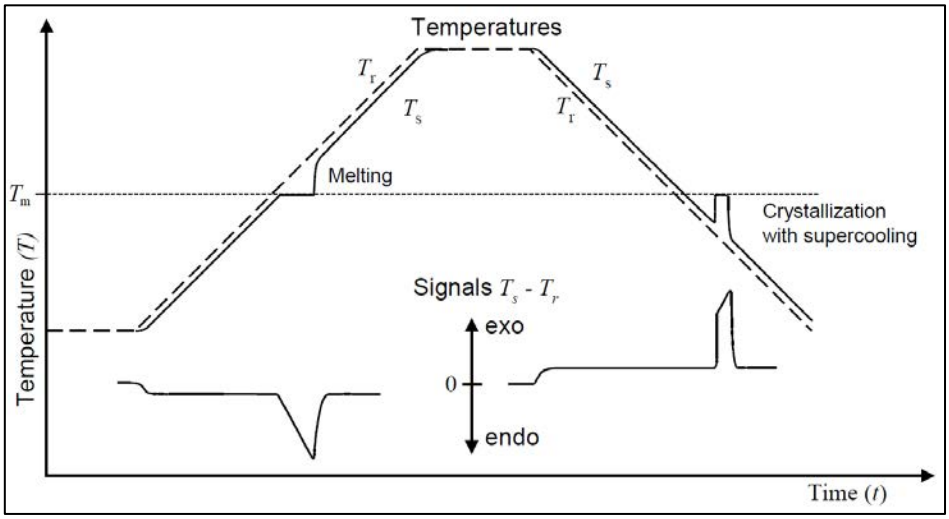

Figure 2-3: *The upper diagram shows the course of the temperatures of sample (Ts) and reference (Tr); the lower diagrams show the resulting signal Ts – Tr*

It is shown that when the material reaches the melting temperature (T_m), during the heating step, the temperature of the sample (T_s) remains constant until all the material under analysis is melted. On the other hand, in the reference crucible nothing happens, so the temperature of the reference (T_r) continues to rise linearly (dashed line). Because of this different behaviour from the sample to the reference, a change in the temperature difference between the two crucibles is caused and a heat flow rate ($d\Delta q/dt \neq 0$) is detected. The resulting signal is shown in the lower part of the diagram: the endothermic peak corresponds to the melting event. In accordance with ICTAC rules, $T_s - T_r$ is positive for exothermic processes (Exo) and negative for endothermic processes (Endo) [37]. During the cooling, the crystallization occurs at $T < T_m$, because of the effect of supercooling.

Through the analysis of the output curves obtained as a result of the conditioning of the sample, a lot of useful information can be gained, by identifying the different points of discontinuity. These make it possible to identify glass transition temperature (T_g), onset and endset temperature (T_{onset}, T_{endset}) for phase transitions. Moreover, the shape of the discontinuity provides information about the kinetics of the transitions. Through the quantification of the height of the different peaks, it is possible to determine the heat absorbed or released by the material and therefore, under conditions of constant pressure, the enthalpy variations related to the different transitions.

2.1.2. Fast Differential Scanning Calorimetry (FDSC)

As discussed in detail in Section 1.2, during the second half of the twentieth century there was a significant development of calorimetry techniques. The origin of this phenomenon can be attributed to the growing interest in the study of appropriate materials, produced and used in conditions far from their thermodynamic equilibrium (e.g. metallic glasses [32, 38]). For the characterization of the structures formed as a result of a specific chemical-physical event, it is necessary to use appropriate analysis methods that allow simulating the real kinetics of occurrences, through the achievement of high scanning rate, especially upon cooling. In this context, Fast Scanning Calorimetry is an attractive tool to study non-thermodynamic equilibrium material. The purpose of this study is to accurately reproduce the trend of the specific heat value of two different aluminium alloy powders, imposing the typical condition of the Additive Manufacturing process. The use

of this technique at high heating and cooling rates will allow achieving results in accordance with the real conditions imposed by this manufacturing method.

2.1.2.1. The Calorimeter

A simplified analytical model will be used to describe the most important features of Fast Scanning Calorimetry, in line with the discussion carried out by Schick et al. [39].

The calorimeter, with the heat capacity C_c and temperature T_c, is surrounded by gas with the temperature $T_{gas} \leq T_c$. The temperature of the calorimeter can be changed by the electric power of the heater P_{el}.

Since the calorimeter is in contact with a gaseous environment at a lower temperature, a thermal flow is generated to the outside environment, as shown in Figure 2-4.

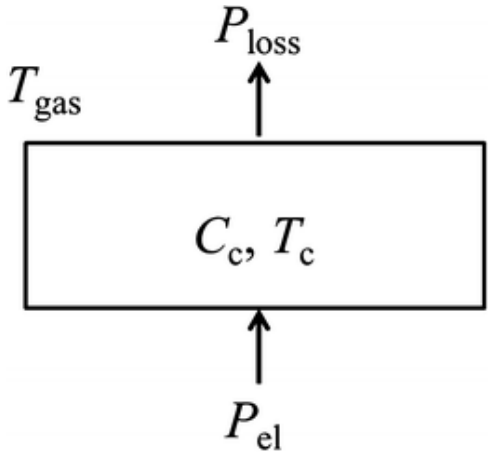

Figure 2-4: *Simplified model of a calorimeter*

The calorimeter loses energy due to this heat flow, P_{loss}:

$$P_{loss} = -\frac{\Delta T}{R_{CG}} \tag{2.1}$$

Where ΔT is the temperature difference between the calorimeter and the surrounding gas ($T_c - T_{gas}$) and R_{CG} is the thermal resistance between the calorimeter and gas, which depends on the type of the gas, the pressure and the size of the calorimeter.

$$P_{el} = -\frac{\Delta T}{R_{CG}} = C_c \cdot \beta \tag{2.2}$$

Where $\beta = (dT_c/dt)$ is the scanning rate.

In order to accurately explain the thermal functioning of the calorimeter, it is convenient to define a heat balance [29]:

$$P_{el}(T) - P_{loss}(T) = (C_c(T) - C(T))\frac{dT}{dt} \tag{2.3}$$

In which C(T) is the heat capacity of the sample.

Important conclusions can be drawn from Equation (2.3):

- For $P_{el} \geq P_{loss}$ the calorimeter is heated or kept isothermal
- The surrounding gas should be at the lowest possible temperature to increase the maximum cooling rate achievable (non-adiabatic mode). It is also possible to reach high rates by increasing the heat conductivity of the gas
- The calorimeter must have a small heat capacity to reach high heating rates. This is possible as long as the volume of the calorimeter is small.

Therefore, the calorimeter usually consists of a thin Si_3N_x – membrane, with the electronic component for heater and temperature sensor.

2.1.2.2. The METTLER-TOLEDO Flash DSC 2+

The commercial instrument of thermal analysis mainly used during the development of this project, is the METTLER-TOLEDO Flash DSC 2+ (Figure 2-5), which allows the achievement of high heating and cooling rates.

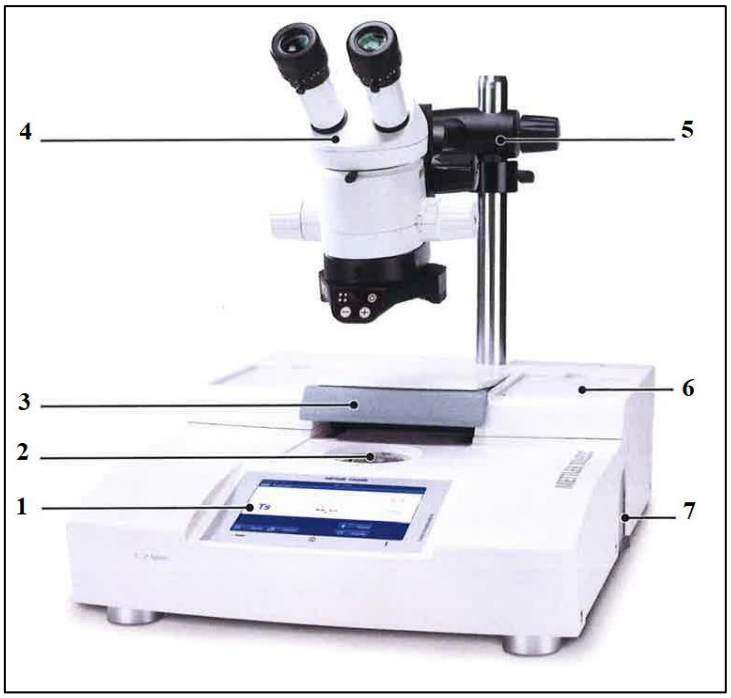

Figure 2-5: *The METTLER-TOLEDO Flash DSC 2+*

1	Touch screen with keys	**5**	Microscope support interface
2	Measuring cell	**6**	Recess for depositing items
3	Insulation lid	**7**	IntraCooler connection
4	Optical microscope		

Table 2.1 *Description of reference in Figure 2-5*

As shown in Table 2.1, the device is also equipped with:

- an optical microscope, necessary to allow the positioning of the sample, of microscopic dimensions, using the bristle of a brush
- an IntraCooler that allows the establishment of non-adiabatic conditions, necessary for specific measurements. This instrument allows reaching a temperature of about -100°C in the surrounding of the sample

– a purging gas (Argon) used to cool the sensor support and to prevent the oxidation at high temperature (not shown).

The implementation of the different measurements at these scanning rates was permitted by using MultiSTAR UFH1 sensors. These sensors are characterized by a time constant smaller than 1 ms, and it is possible to run experiments using scanning speeds that extend from 0.5 to 40,000 K/s (30 - 2,400,000 K/min). Thanks to the use of these devices, it is possible to carry out measurements in a wide heating and cooling rate range, beyond the maximum scanning rate limit of conventional DSC. The Flash DSC, therefore, complements a conventional DSC, making accessible a heating and cooling rate range of more than seven decades, with the combination of both instruments.

The region in which the thermal analysis is physically conducted is located under the sliding lid, which allows the isolation of the sample from the external environment. In this area is fitted the support for the sensor, consisting of a set of pins (Figure 2-6) that allow contact between the measuring instrument and the sensor itself. The electrical contact has been improved using a suitable clamping disk, that fixes the position of the sensor on the instrument. The volume of the furnace is approximately $4x10^{-13}$ m^3, the density is circa 3.2 g/cm^2 and the specific heat capacity is 0.5 J/g·K. This means that the heat capacity of the furnace is circa 600 nJ/K.

Figure 2-6: *Positioning of UFH 1 Sensor on the sensor support with pins contact*

The several thermal analysis programs performed by the Flash DSC 2+, are implemented by STARe Software that is directly provided by Mettler Toledo. This software allows the creation of different thermal programs, customized according to the needs of analysis, through the implementation of up to 200 segments. The same software also makes it possible to use sensors with different technical characteristics. Furthermore, STARe provides a lot of different evaluation and correction options on the output curve including temperature corrections with reference, integrations, measurements of onset and endset temperature.

2.1.2.3. Sensor design

For all Fast Differential Calorimetry measurements carried out on the different samples, MultiSTAR UFH1 sensors from Mettler Toledo were used. The sensor UFH1 is a non-adiabatic chip calorimeter, embedded in ceramic support, based on MEMS technology (MEMS: Micro-Electro-Mechanical System). They consist of two different calorimeters, one used for sample positioning and one for the reference. This characteristic makes them very similar to the conventional DSCs, in terms of operating mode, even if there is not a real crucible: the sample is just positioned on the calorimeter to run the experiment.

The twin calorimeters are composed of two different layers: the first one is constituted by silicon nitride membrane with a length of 16 mm, while the second one, placed on the underside of the membrane, is made of Silicon oxide. The total thickness of the membrane is 2 µm. They are mounted on a Silicon frame; which thickness is 300 µm. The sample area, with a diameter of 0.1 mm, is in the middle of the membrane and it is coated with Aluminium; this works as heater and allows to achieve a more homogenous temperature profile on the calorimeter and then on the sample.

In Figure 2-7 [49] it is possible to appreciate the different parts of the measurement sensor.

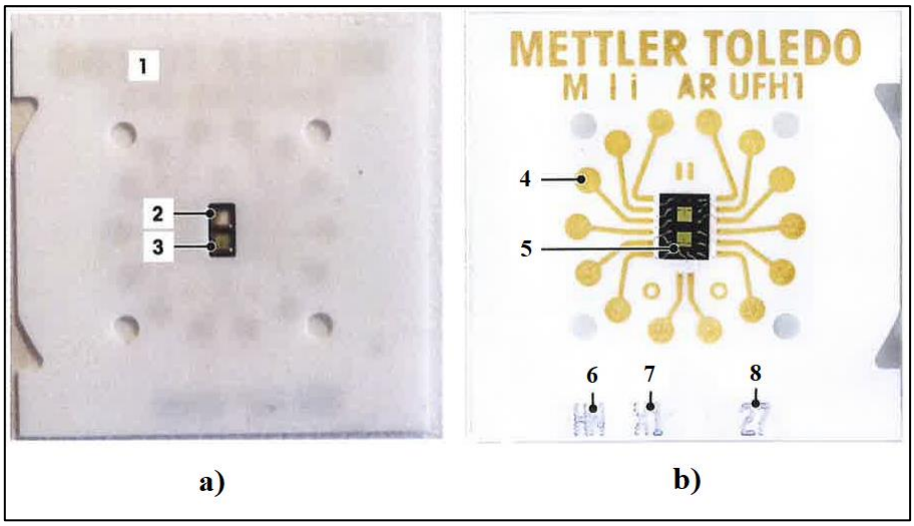

Figure 2-7: *Chip Sensor TOP (a) and BOTTOM (b)*

1	Ceramic plate (substrate)	**4**	Contact pins
2	Sample side	**5**	Type
3	Reference side	**6**	Year of manufacturing
		7	Serial number

Table 2.2: *Description of references in Figure 2-7*

Note the presence of an alphanumeric digit on the lower portion of the Silicon support. This is the serial identification code of the sensor itself and will, therefore, be present on every micro-chip. Also, the gold contact points are visible around the membrane; half of them are necessary for the heating, and half for monitoring temperature.

A more detailed cross-section representation is shown in Figure 2-8.

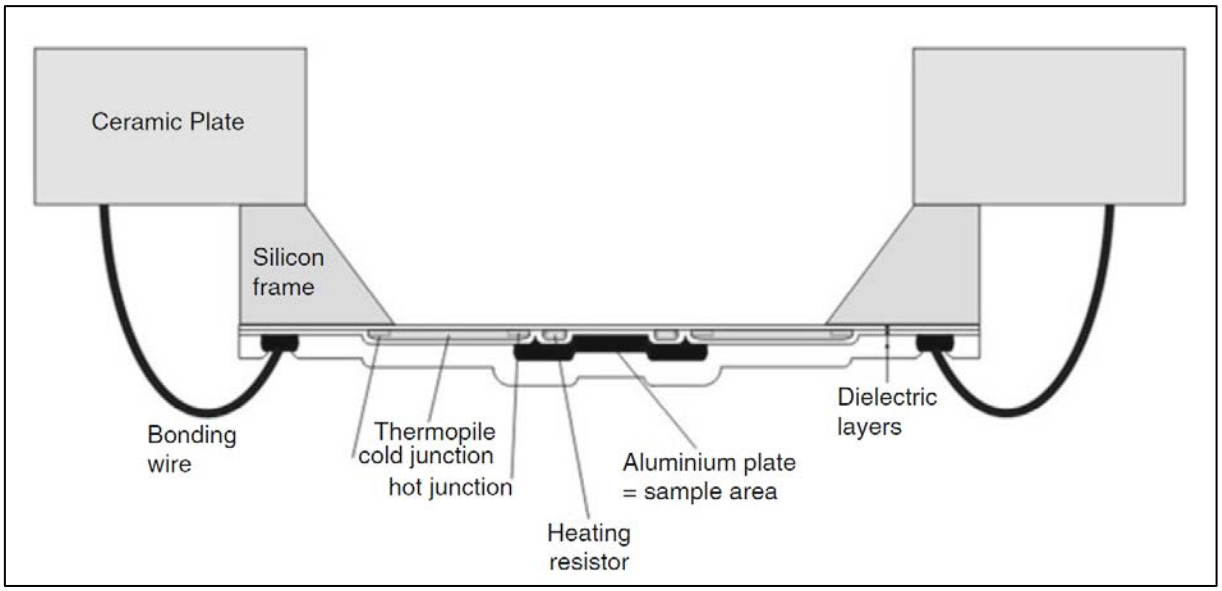

Figure 2-8 *Schematic representation of UFH 1 Sensor profile*

Looking carefully at the sensor profile, the position of the individual layers, the measurement area covered by an Aluminium coating and the presence of the heating resistor adjacent to it can be seen. The electrical connection between the Silicon frame and the ceramic plate is made by a bonding wire.

2.1.2.4. Measuring principle of Flash DSC 2+

The use of UFH 1 sensors with their two independent furnaces, means that the Flash DSC 2+ operates in a true power-compensated mode, so the temperature difference between the furnaces is kept to zero by modulating the amount of power. This is made possible by the excellent symmetry of the sensor obtained from the micro-fabrication process.

The temperature measurement system is based on the presence of eight thermocouples on the sensor, which measure the temperature of the sample and the reference. The temperature of sensor support (T_{ss}) is used as a reference temperature for the cold junction. T_{ss} is also the temperature of the surrounding gas, which flows on both sides of the sensor. In practice it is always necessary to wait a certain time to reach the equilibrium between the gas temperature and the temperature of the sensor support. The sensor support temperature T_{ss} has three different stages: “power off”, “standby temperature” and “ready temperature”. In the state “power off” the reference temperature is not

controlled, so the sensor support reaches the minimum temperature set by the cooling device. The standby and ready temperature can be defined through the module window of STARe. Generally, the standby temperature should be selected between 10 and 40 °C. When T_{ss} equals the standby temperature, the sensor can be exchanged, and the sample can be positioned. If T_{ss} is equal to the ready temperature, the so-called correction procedure can be performed.

2.1.2.5. Placing sensor

The procedure for the installation of the sensor on the holder of measuring instrument is an operation to be performed with the greatest possible care and accuracy, in order to avoid the occurrence of problems during the analysis. According to *"Fast Scanning Calorimetry"* [39], it is appropriate to follow a series of fundamental steps:

1) Selection of the ready and standby temperature in the installation window of the software. The ready temperature should be selected only if the instrument is ready for the measurement. The lower the ready temperature, the higher the cooling rate achievable. But, the lower this temperature is, the higher the time necessary to stabilize the temperature before the measurement.
2) Identification of the sensor ID and clamping the sensor on the support, verifying an appropriate electrical contact with the pins. Afterward, the conditioning procedure can be performed, where the behaviour of the sensor can be checked. The conditioning can be carried out when the sensor support temperature is stabilized at the standby temperature. The program should be run once however in this study it was chosen to run four times. If the Flash DSC 2+ is connected to an IntraCooler, it must be switched off during the conditioning, and for at least 5 hours before, in order to have the whole machine in thermal equilibrium with its surroundings.
3) Performing the correction procedure with closed insulation lid. This process is performed in order to correct the signal of the thermocouples with respect to the cold junction temperature (T_{ss}). The sensor support temperature for the various analyses has been set to -90°C. Before performing the correction, it is necessary to wait until T_{ss} has reached equilibrium at the ready temperature. The

thermocouple correction parameters are stored for each chip sensor in the STARe Software database.

4) Heating the sensor support temperature to the standby temperature once the correction is finished, and opening the lid.
5) Placing the sample on the sensor. In order to perform the thermal analysis it is recommended to pre-melt the sample to ensure greater thermal contact with the sensor. A glass plate should partially cover the sensor housing.
6) The lid can be closed, and the temperature can again be set at ready temperature. When the ready temperature is equal to T_{ss}, it is possible to start the measurements.

2.1.2.6. Temperature program

The thermal measurement involves the definition of an appropriate temperature program, in order to analyse the behaviour of the material as the temperature and the scanning rate vary. The implementation of this schedule is carried out through the "Method window" of STARe. Generally, the thermal program consists of several temperature segments with alternating cooling and heating segments. The insertion of short isothermal steps between two different dynamic segments is strongly recommended in order to ensure the target temperature is achieved. Longer durations are avoided in order to prevent the occurrence of phenomena, particularly metallographic, which may cause significant variations in the sample. However, long segments (isothermal or low scanning rates) may be used to establish a desired sample state. These segments are applied at the beginning of the thermal program, and usually are not evaluated. In some case the sample may change its behaviour during FSC measurements, e.g. due to non-reversible physical or chemical transformations. To recognize such effects, in Fast Scanning Calorimetry [39], it is recommend to implement several segment sequences which can demostrate the repeatability of a sensitive thermal event. If the measured curves of the test segments are not reproducible, the sample has been irreversibly changed.

2.1.2.7. Sample preparation for Flash DSC

As described previously, after the sensor has been mounted in the appropriate housing and the condition and correction procedure have been carefully carried out, the sample is placed on the furnace area in the middle of the sensor. In most of the experiments performed, being metallic powders, the positioning of the sample was performed using a brush bristle or a simple hair, properly cleaned to avoid electrostatic attraction with the micrometric sample. If it was necessary to take the sample from a larger piece, a scalpel was used.

For a correct Flash DSC measurement, the selected samples must have specific dimensional characteristics. These dimensions are such that they can be positioned inside the sample area located in the middle of the sensor, with a diameter of about 100 μm, as shown in Figure 2-9.

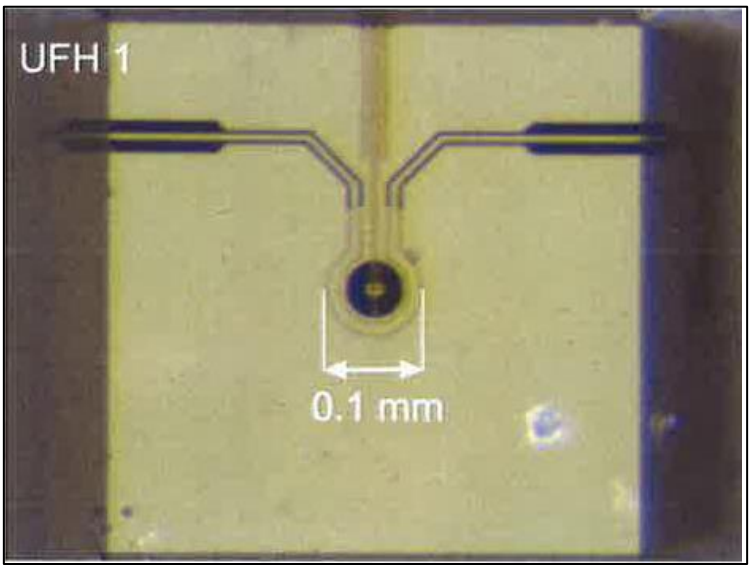

Figure 2-9: *Sample area on the UFH 1-type chip sensor membrane*

In this way it is possible to achieve the best homogeneous heating. The use of samples with dimensions exceeding the maximum limit, besides not allowing their insertion in the sample area, would cause difficulties in cooling the sample at high rates, without thermal lag in the signal. On the other hand, the smaller is the sample size and the weaker is the signal given by the instrument. The samples should also have an almost flat shape and

not too high thickness, in order to allow good thermal contact with the sensor and to minimise temperature gradients within the sample.

In the case of high scanning rates, the sample size should be small. Moreover, if the sample size stays below a material-specific limit, the measured effects are size dependent due to surface-induced processes. For slow rates, larger samples should be used. However, distortions of the measured signal can then be generated (smearing of the curve), due to the influence of dynamic temperature gradients.

For almost every experiment, the size of the sample under analysis is an essential parameter to be evaluated. The sample mass (m_{FDSC}) can be analytically calculated, by determining the enthalpy of fusion.

$$m_{FDSC} = \Delta H_m \cdot \frac{A_r^s}{\Delta H_{fus}^s} \quad (2.4)$$

Where ΔH_{fus}^s (in kJ mol^{-1}) is specific enthalpy of fusion determined by conventional DSC measurements, ΔH_m (in kJ) is the enthalpy of melting obtained from integrating the measured Flash DSC curve and A_r^s (in g mol^{-1}) is the molar mass of the material.

2.1.2.8. Heat flow signal analysis

As treated in Section 2.1.1, the analyses in the conventional DSC are carried out by conditioning to the same thermal program, the sample contained in a crucible, of heat capacity C_s, and an empty crucible (C_R) on the reference side. Since the heat capacity of the sample is significantly smaller than that of the furnace, the behaviour of the latter can be widely corrected for and removed from the measured curve simply by subtraction of the blank curve [35]. This curve can be obtained by a measurement performed using an empty crucible on the sample side, of heat capacity C_s.

For Flash DSC measurements the situation is completely different, due to a different influence of the sample on the measuring system. As observed by Pogatscher et al. [40] during studies related to the bulk behaviour of a gold-based bulk metallic glass alloy, the heat capacity of the sample is in the order of the heat capacity of the active zone of the

sensor. Consequently, the empty sensor cannot be used as a blank curve. Because of the large temperature difference between the hot sensor and the cold surrounding gas, the thermal losses between sample and reference side of the calorimeter cannot be completely compensated. Thus, the measured heat flow can be described by:

$$\Phi = m \cdot c_p \cdot \beta + \Phi_1 \quad (2.5)$$

Where m is the sample mass, c_p is the specific heat capacity of the sample, β is the heating rate and Φ_1 is the heat loss function, which is in good approximation independent of the scanning rate. Starting from Equation 2.6, it has been possible to identify two different methodologies that allow the evaluation of the heat loss function, and thereby to determine the actual heat flow into the sample [41].

Through the first method, it is possible to evaluate the heat loss function using a low heating rate. In this way, the heat flow contribution due to the heating of the sample can be neglected, and the measured heat flow is approximated to the loss function (Equation 2.6).

$$\Phi_{\beta \to 0} = \Phi_1 \quad (2.6)$$

Because of the use of low scanning rate to allow the sample term to be overlooked, this method is called *slow-rate correction*. For the implementation of this procedure, it must be observed that the heat losses are not necessarily the same on heating and cooling. Therefore, the *slow-rate correction* is applied separately for heating and cooling.

On the other hand, at high heating rate the contribution of the heat loss function to the measured heat flow will be relatively small, which means that the measured heat flow resembles more closely the sample heat flow.

The second method uses the average heat flow between heating and cooling, to determine the heat loss function. For this reason, it is called *symmetry correction*.

$$\Phi_{avg} = \frac{\left(m \cdot c_p \cdot \beta + \Phi_{1,h}\right) + \left(m \cdot c_p \cdot (-\beta) + \Phi_{1,c}\right)}{2} \quad (2.7)$$

$$\Phi_{avg} = \frac{\Phi_{1,h} + \Phi_{1,c}}{2} = \Phi_1 \quad (2.8)$$

Where $\Phi_{1,h}$ and $\Phi_{1,c}$ are the heat loss function for heating and cooling measurement, respectively.

Finally, it is pointed out that the determination of the heat flow into the sample, by subtracting the heat loss function obtained by one of the two correction methods, allows the evaluation of specific heat capacity of the material.

2.2. Scanning Electron Microscopy

The Scanning Electron Microscope, or more briefly SEM, is a type of electron microscope that produces images of the sample under analysis, through the scanning of the surface with a focused beam of electrons. In function of the level of the interaction between the high-energy electron beam and the atoms making up the sample, secondary electrons, backscattered electrons, Auger electrons and X-rays can be generated. Following their detection, these signals allow evaluations of:

- Morphology of the sample surface
- Chemical-physical composition
- Electrical defects
- Surface contamination
- Superficial potentials

A JSM-IT 300 LV by Jeol shown in Figure 2-10, is used for the analyses of the different powders.

Figure 2-10: *A JSM-IT 300 LV by Jeol Scanning Electron Microscope*

2.2.1. Operating principles

As shown in Figure 2-11, a beam of electrons with kinetic energies between 1 and 30 KeV, called primary electrons, is generated by an electron gun placed at the top of the working column. The gun itself is the cathode of the measuring system. The sample is mounted on a stage in the chamber area; both the column and the chamber are evacuated by a combination of pumps. The level of the vacuum depends on the design of the microscope. The electron beam is attracted towards the anode and focused on the massive sample, through a system of objective lenses. The thickness of the test sample is such that it is not completely penetrated by the incident electrons. As a result of the collision between the electron beam and the sample, different signals can be produced including X-rays, Auger electrons, secondary electrons and backscattered electrons. These electrons are then collected by appropriate detection systems, depending on the type of signal to be analysed.

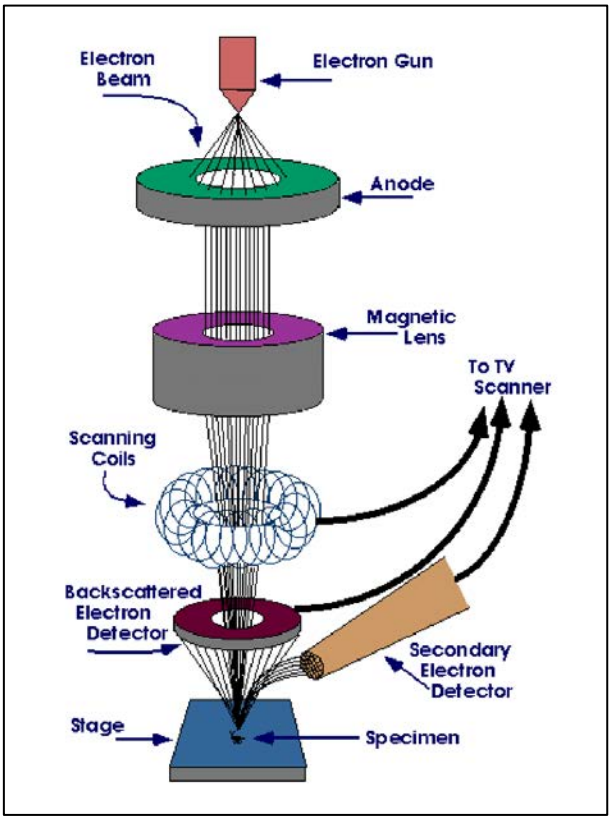

Figure 2-11: *Schematic representation of a Scanning Electron Microscope*

2.2.2. Energy Dispersive X-ray Spectrometry

An element that contributes to the versatility of the SEM, is the possibility to obtain images through the different radiation emitted by the sample, once exposed to primary electrons. Using the detection of secondary and backscattered electrons, the morphology of the samples can be analysed. Through the analysis of X-rays, it is possible to evaluate the composition of the sample, since the energies of the emitted X-rays are characteristic of the atoms from which they come.

A characterization technique that exploits the emitted X-rays is the Energy Dispersive X-ray spectroscopy (EDS or EDX). When incident electrons collide with the sample under analysis, the electrons present in the inner shell of the atoms can be ejected from the atoms themselves or promoted to higher energy levels. In this second case, electron vacancies will originate in the innermost levels, which will then be filled by electrons from the outer shells. The transition of an electron from a higher energy shell to the electron vacancy causes the emission of X-rays, which energy is equal to the energy difference between the two electrons state. The energy of the X-ray is characteristic of the element from which it originates. In general, the emitted X-rays are detected by a Si(Li) solid-state detector. When the X-rays hit this detector a charge pulse, proportional to the energy of the ray, is generated. The charge pulse is then converted into a voltage signal. An analyser collects all the signals from the detector, and it sorts them by voltage. Then the data are plotted in an EDS plot; the spectrum of X-ray energy versus counts is evaluated to determine the elemental composition of the sample.

3. Materials

In this chapter, following a brief description of the properties of metal alloys as they vary in composition, the different reasons that lead to the use of AlSi10Mg and Scalmalloy® in the AM technique are explained. Subsequently, the results obtained from the EDS analyses carried out on the two types of aluminium alloys are reported.

3.1. General characteristics of Aluminium Alloys

High-purity aluminium (i.e. with a minimum aluminium content of 99.50 %) is a silvery-grey metal, with a face-centred cubic crystalline structure. This metal material is characterized by low density values (2700 kg/m^3), a melting point of 660 °C and excellent characteristics of plastic deformability and weldability. However, the mechanical properties of pure aluminium are rather low, with unit tensile strength of 60-100 MPa and elastic modulus (E) of about 70,000 MPa. Because of its poor mechanical properties, the use of pure Al at industrial levels is reduced to a few special cases.

Over the years various techniques have been introduced in order to improve the mechanical characteristics of pure aluminium. For example, an improvement treatment often used in this field is the so-called hardening by plastic deformation. Nevertheless, the industrial use of this metal remains very limited, unlike the corresponding aluminium alloys. The addition of alloying elements, such as copper, manganese, silicon, magnesium and zinc considerably improve the tensile strength, which can exceed that of mild steels. However, in some cases, other properties may deteriorate, as shown in Table 3.1.

	Cu	Mn	Si	Mg	Zn
Mechanical properties	↑↑	↑	↑	↑	↑
Cold deformability	↓	↑	↓	↓	↓
Corrosion resistance	↓	↑	=	↑	=
Weldability	↓	↑	=	↑	↓

Table 3.1: *Effect of the main alloying elements on the mechanical strength, cold deformability, corrosion resistance and weldability of pure Aluminium*

Among the various alloying elements listed, some of them allow the achievement of high mechanical performance as a result of implementing the appropriate heat treatments. Generally, common heat treatments on an aluminium alloy consist of three phases of operation:

1) Solubilisation treatment: involves heating between 450 °C and 500 °C, so that most of the alloying elements are dissolved in the aluminium matrix.
2) Rapid quenching in water: a solid aluminium solution is obtained, which is over-saturated with the alloying elements.
3) Low temperature ageing: precipitation of intermetallic compounds, consisting of aluminium and the present alloy elements, which are finely and homogeneously dispersed in the aluminium matrix.

The precipitation of these intermetallic elements act as obstacles to dislocation movements, leading to an increase in the mechanical performance of the alloys.

It can be observed that heat treatment is very similar to the deposition process, layer-by-layer, characteristic of Additive Manufacturing. This condition, added to the low specific weight and good weldability that the different aluminium alloys generally have, makes them suitable for producing mechanical components with this manufacturing technique.

3.2. Analysed Aluminium alloys

3.2.1. AlSi10Mg alloys

Among commercial aluminium alloys, mainly near eutectic Al-Si alloys are used in Additive Manufacturing processes. Among them, the most studied composition for this technique is certainly AlSi10Mg. This alloy offers a low melting point, good weldability, low density and improved mechanical properties after thermal treatment. All these characteristics are attributed to the composition of the alloy, which defines its great success in the field of AM. This specific composition is located at the hypoeutectic region of the Al-Si phase diagram, close to its eutectic point. The near-eutectic composition reduces the solidification cracking[1] phenomenon. This phenomenon is dependent on the solidification range of the alloy, on the fluidity of the molten phase and on coefficient of thermal expansion (CTE) of the alloy [42]. The presence of 10 wt. % Si implies a fine solidification range ($\Delta T = T_{Liquidus} - T_{Solidus}$) of the alloy, which was calculated to be about 30°C. This narrow solidification range permits tighter dimensional control for building complex shapes structures [43]. In addition, it is well-known that silicon improves the fluidity of molten aluminium, reduces the solidification shrinkage and the coefficient of thermal expansion. Furthermore, according to the studies conducted by Sercombe et al. [44], it has been suggested that silicon is the responsible for the laser absorption, which is fundamental for the LPBF process (see Section 1.1). In fact, this element has low solubility in Al and it is mainly contained in the alloy as pure particles which cause the higher laser adsorption.

3.2.1.1. Composition and morphology of AlSi10Mg powder

The AlSi10Mg alloy powders used for the different measurements were produced by inert gas atomisation. This method is the one most used to obtain metal powders, whereby molten metal is pushed through a nozzle of restricted dimensions, and atomized through an inert gas, such as argon or nitrogen. The flow of inert gas allows the metal to cool and solidify, and the resulting particles are collected at the bottom of the processing chamber.

[1] The solidification cracking constitutes a defect in some metallic materials, which originates from the formation of shrinkage cracks, during the solidification of weld metal.

In order to evaluate the composition and morphological characteristics of the powders, analysis by Scanning Electron Microscope was implemented. Portions of the powders under analysis were glued, by means of a graphite scotch tape, on to sample-holders which were then mounted inside the measuring chamber.

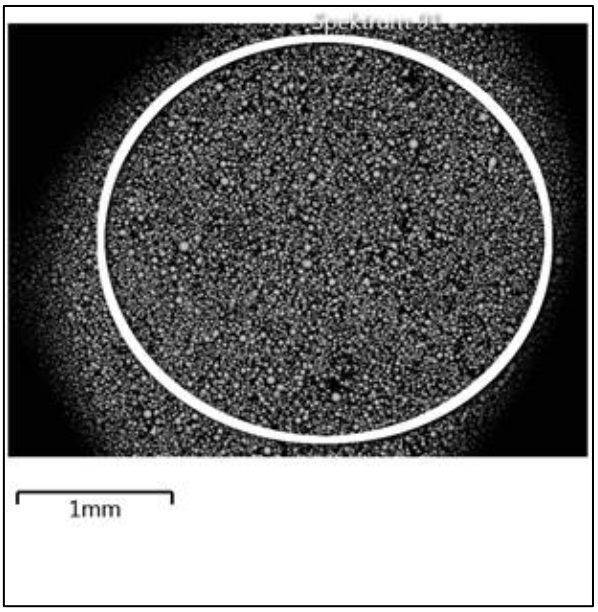

Figure 3-1: *SEM image of AlSi10Mg powder*

Figure 3-1 shows an image obtained by SEM of a localized region of powder, adhered to the sample holder. Subsequently, an EDS analysis was performed to evaluate the composition of this portion of powder (Figure 3-2).

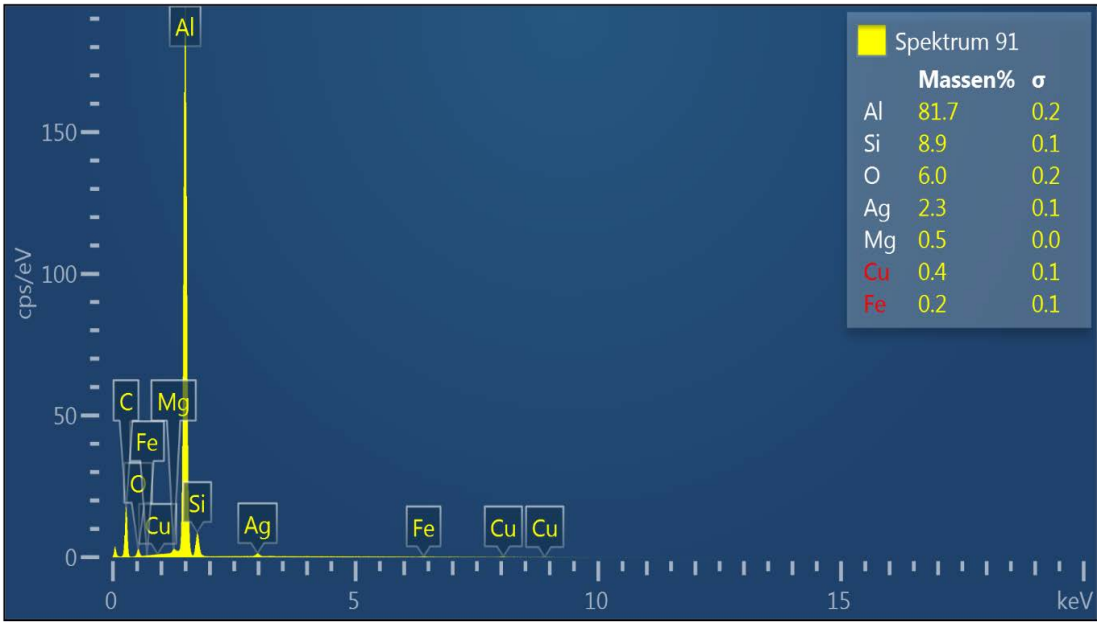

Figure 3-2: *EDS spectrum of AlSi10Mg powder analysed*

As it can be observed from the EDS spectrum, the main elements that compose the portion of analysed powder, are aluminium (main constituent with 81.7%), silicon (8.9%) and magnesium (0.5%). This composition is very similar to the values found in the literature where this powder is used in LPBF processes. Of course, in the overall evaluation of the result, the intrinsic uncertainties of the microscope itself must be considered.

In addition, it is necessary to observe the presence of a non-negligible amount of oxygen, probably due to non-optimal procedures for powder maintenance. Even in this case, the compositional value is not to be considered perfectly in line with reality. Often, the oxygen signal is confused with that of other elements, characterized by similar counts. For this reason, it was decided to carry out additional measurements, using a higher level of zooming and accuracy.

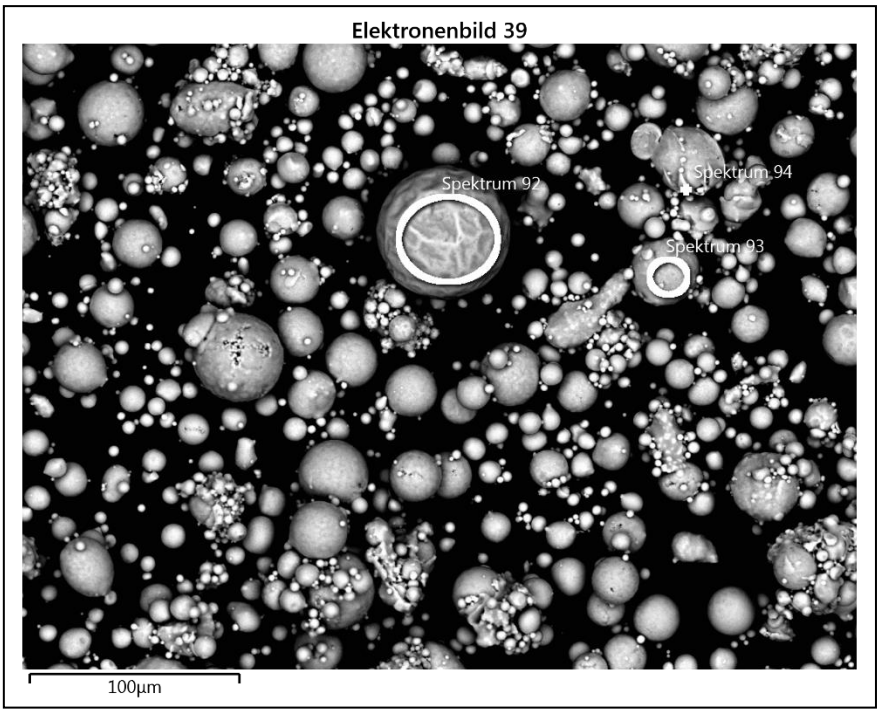

Figure 3-3: *SEM image of AlSi10Mg (higher magnification)*

Figure 3-3 shows a more magnified image of the AlSi10Mg powder portion. It can be observed that, for the purpose of the analysis, three different metal powder particles have been identified. An EDS analysis was then performed, for each particle.

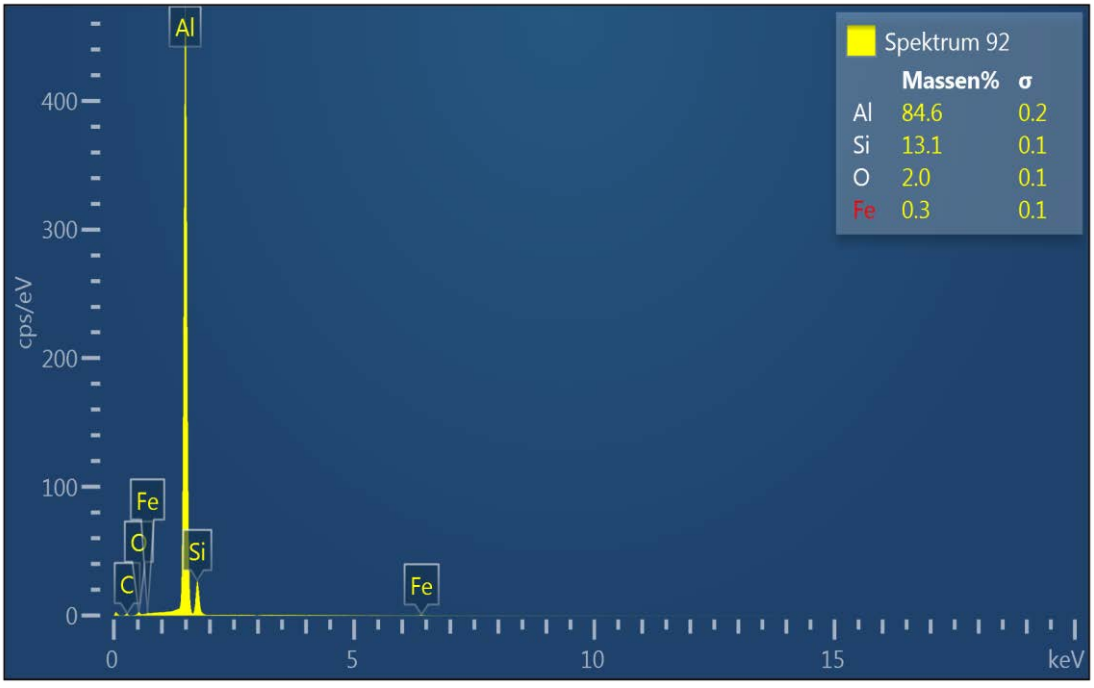

Figure 3-4: *EDS spectrum of AlSi10Mg powder analysed (Spektrum 92)*

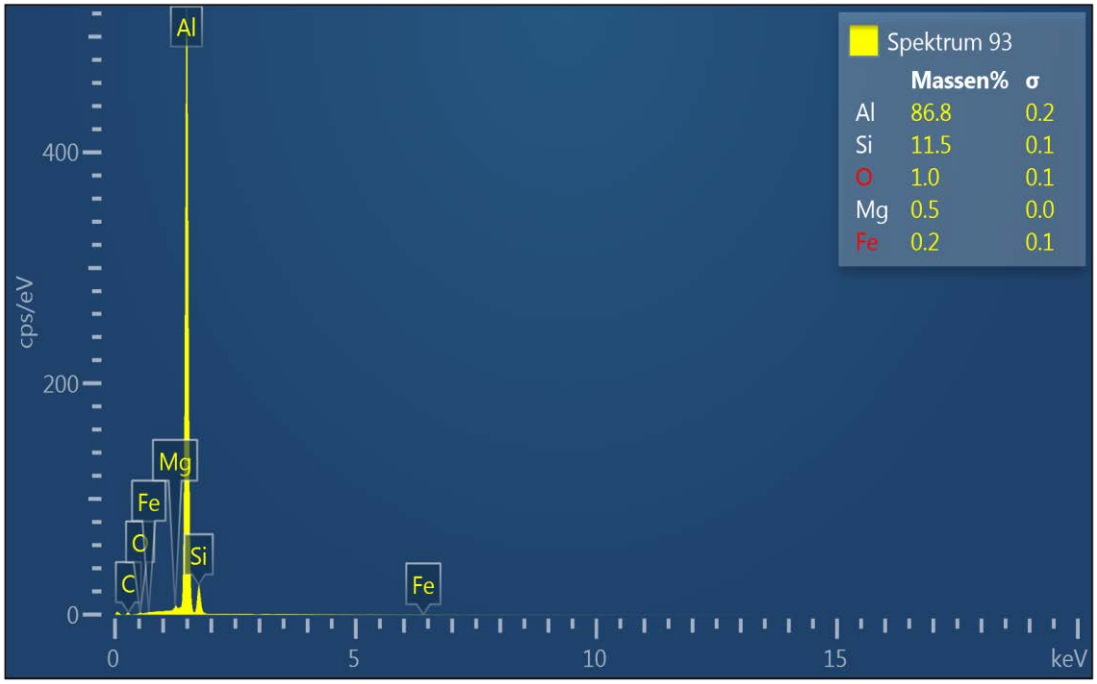

Figure 3-5 *EDS spectrum of AlSi10Mg powder analysed (Spektrum 93)*

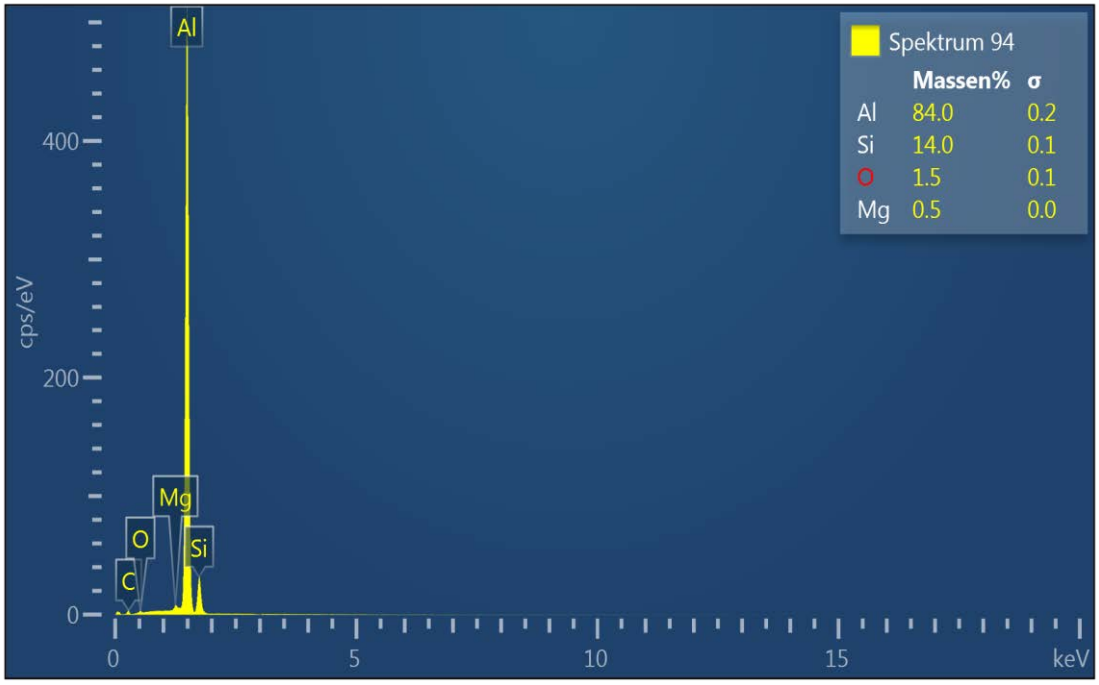

Figure 3-6 *EDS spectrum of AlSi10Mg powder analysed (Spektrum 94)*

It is shown that for all three particles the amount of Oxygen is still significant, confirming more of its presence in the overall composition. This observation is further confirmed with a mapping procedure, performed on the same region shown in Figure 3-3.

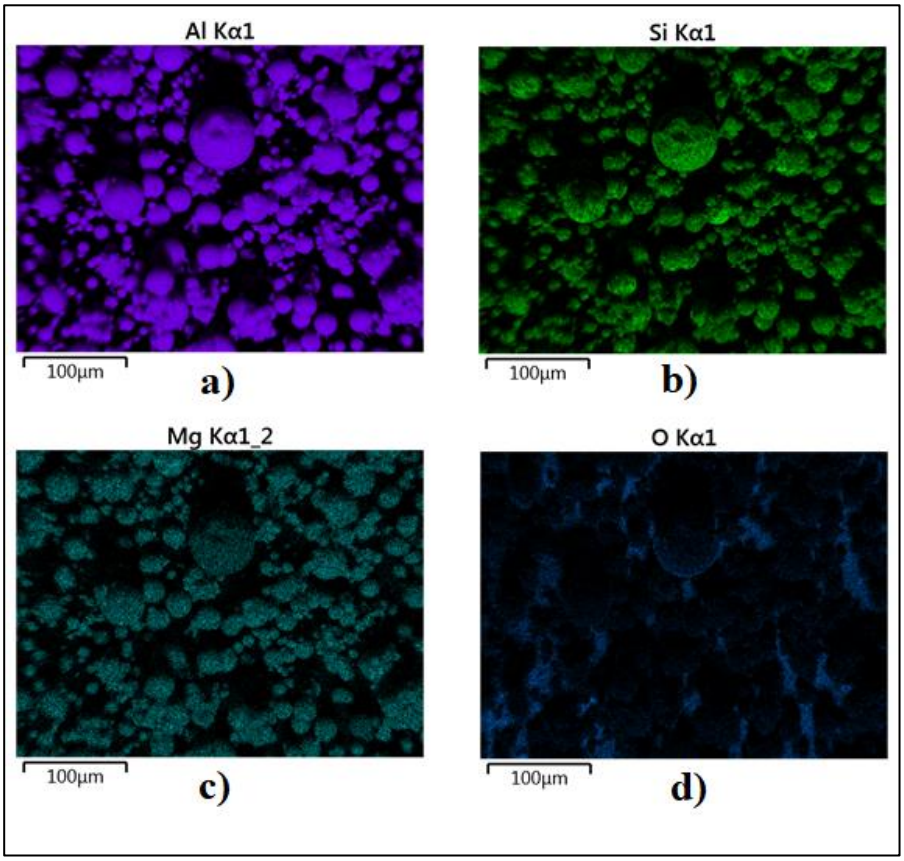

Figure 3-7: *Compositional distribution of Aluminium (a), Silicon (b), Magnesium (c) and Oxygen (d)*

3.2.2. Scalmalloy®

The use of specific alloy elements has allowed obtaining high-performance aluminium alloys, in which the high lightness of the base material is combined with the high mechanical performances reached by alloying. However, the high mechanical performance of a given alloy is not the only necessary condition for its use in 3D printing; high plasticity, as well as good corrosion and fatigue resistance, has to be guaranteed. Silicon for example is one of the most used elements for the production of alloys suitable

for this kind of process, especially for reaching significant improvements in mechanical properties. However, as seen in Table 3.1, the addition of this element leads to a decrease in cold deformability.

Over the last few years, a different approach for the obtaining new Al-based compositions has been developed by introducing transition metals or rare earth elements to the alloy compositions. Among these types of elements, those most used especially in SLM process are Scandium and Zirconium, which led to the development and patent by Airbus Group of the high performance material, Scalmalloy®.

The great success of Scalmalloy® in Additive Manufacturing is attributed to the considerable improvement in mechanical performance resultant from small additions of scandium and zirconium. Furthermore, it has been demonstrated that the strengthening potential can be improved by increased cooling rate [45-46]. During SLM process, the solidification rate within the molten pools can go up to 10^4-10^6 K/s, facilitating the trapping of more scandium in solid solution. After a subsequent ageing treatment, the decomposition of the supersaturated scandium in aluminium matrix leads to the formation of large quantities of nano-size precipitates (Al_3Sc), promoting the possibility of precipitation hardening. On the other hand the primary Al_3Sc precipitates act as heterogeneous nucleation sites for grain crystallization. Refining the crystalline grain is very desirable for SLM processes since it can improve intergranular liquid feeding and accommodate strains generated during the rapid solidification [4].

3.2.2.1. Composition and morphology of Scalmalloy® powder

The Scalmalloy® powder used in the different analyses is produced using inert gas atomisation. Table 3.2 shows the initial composition coming out of the atomizer, supplied by the manufacturer.

Chemical element	Al	Mg	Sc	Zr	Mn
Concentration (ppm)	93.92%	4.6%	0.66%	0.42%	0.4%

Table 3.2: *Initial composition of Scalmalloy® powder*

It is important to underline that the powders analysed are those commonly employed in SLM processes for the production of various components, and that mechanical resistance is among the most essential characteristics for final piece. As mentioned above, this characteristic can be obtained by adding even small amounts of Scandium, as shown in Table 3.2 (0.66%).

Also for Scalmalloy powder, it was necessary to evaluate the morphology and composition, essential characteristics especially for the carrying out of the production process. As with the AlSi10Mg powder, Scanning Electron Microscope was used for these analyses. The sample mounting procedure and the sampling method adopted are the same, as those described for the first type of powder

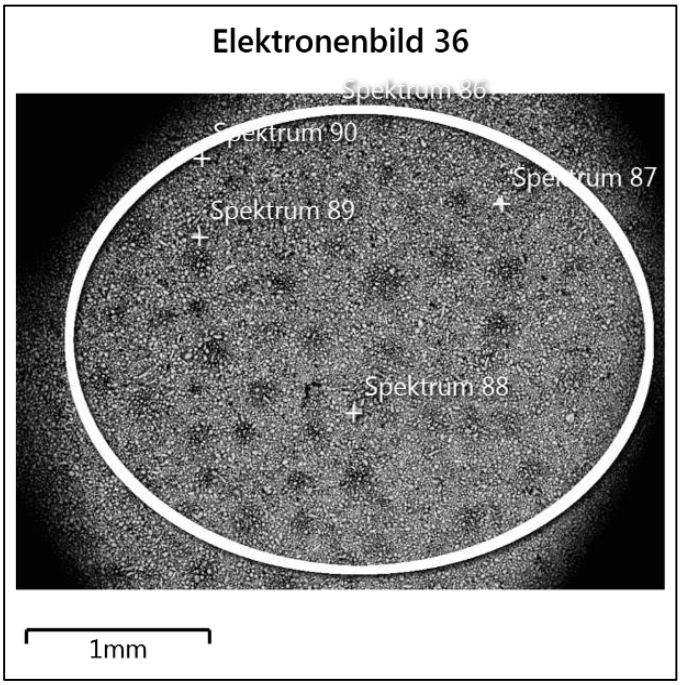

Figure 3-8: *SEM image of Scalmalloy powder*

Figure 3-9 shows the EDS spectrum obtained from a global analysis of a given portion of sampled powder. It can be seen from the relative table, how the Scalmalloy® powder is mainly composed of aluminium (main constituent with 88.4%), magnesium (4.5%), scandium (0.7%) and manganese (0.6%). These elements are present with a percentage very similar to the initial composition provided.

Among the main constituents detected by the SEM, zirconium is not present, despite being one of the two transition metals that characterizes this powder. Its absence in the spectrum could be due to a too-small amount of this element, or, more likely, interference of its characteristic peak with that of another element. Also in this powder a moderate amount of oxygen is observed in the overall composition, the presence of which can be traced back to the same causes mentioned in §3.2.1.

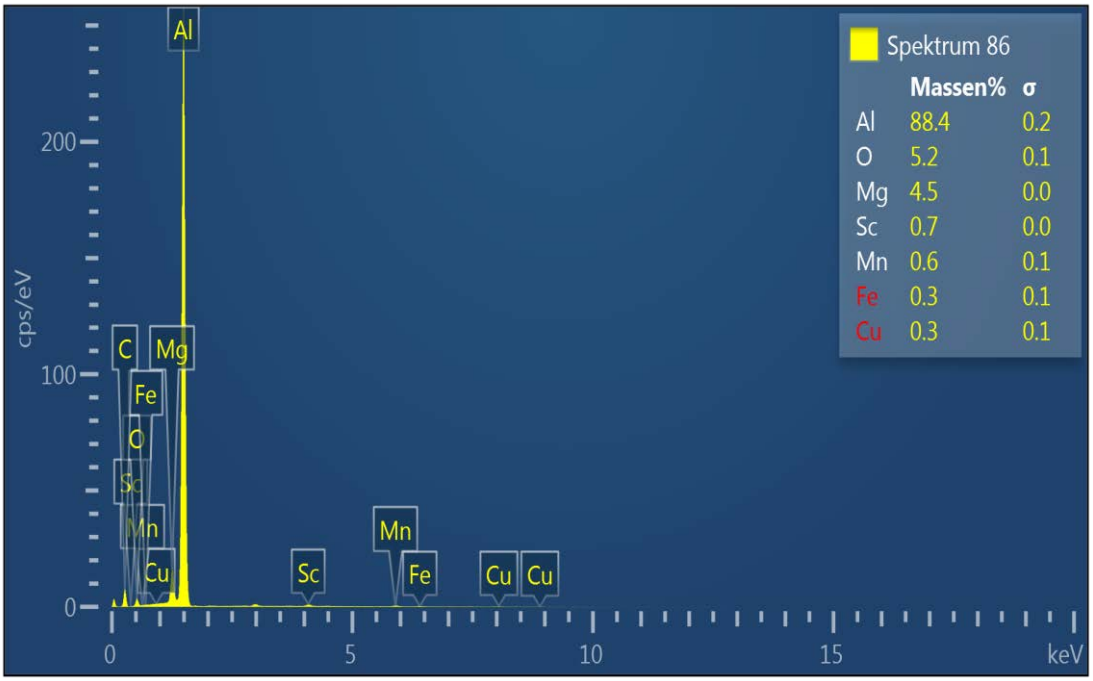

Figure 3-9: *EDS spectrum of Scalmalloy® powder analysed (Spektrum 86)*

In this case, it was again considered necessary to perform a more accurate analysis on the portion of powder, through the determination of three localized regions (Spektrum 88, Spektrum 89 and Spektrum 90).

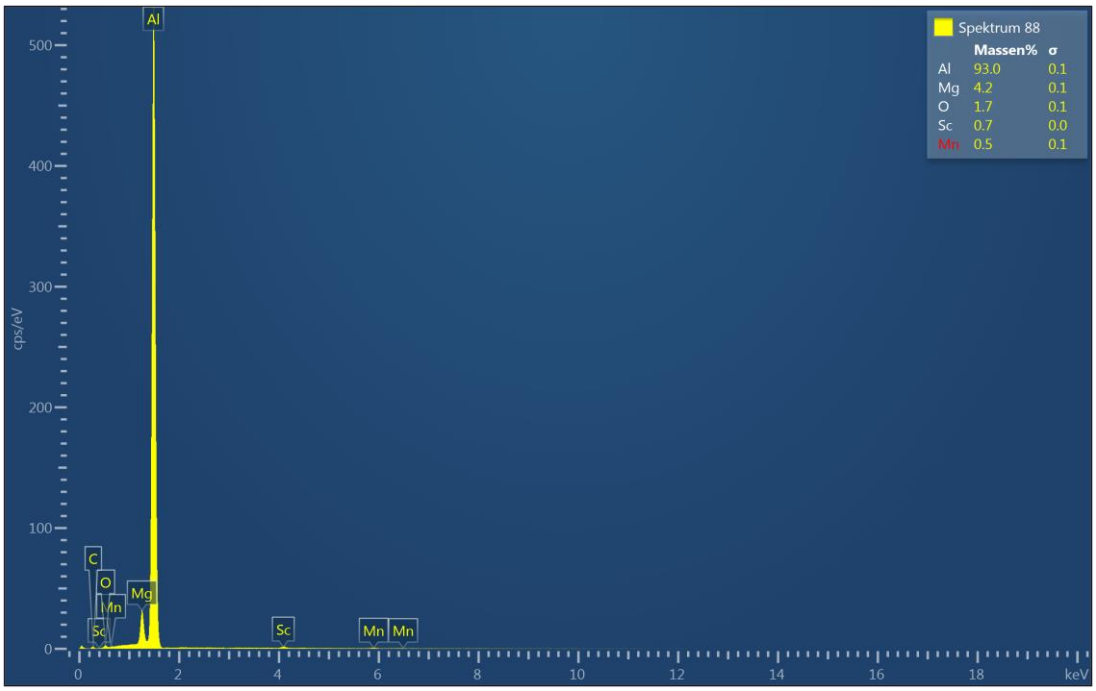

Figure 3-10: *EDS spectrum of Scalmalloy® powder analysed (Spektrum 88)*

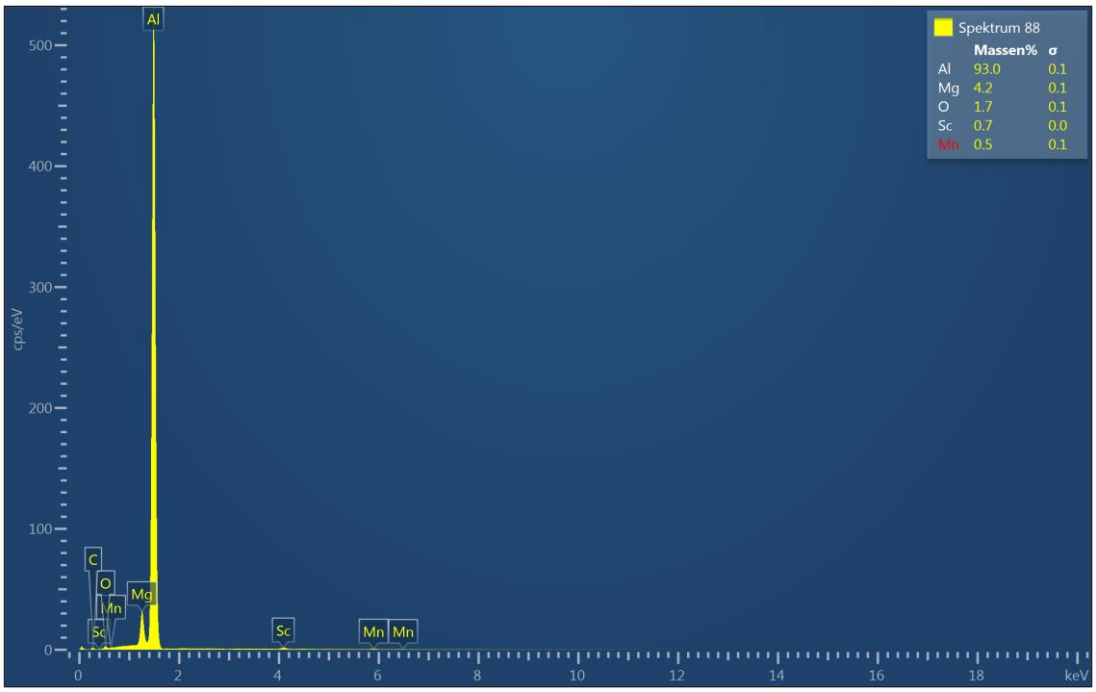

Figure 3-11: *EDS spectrum of Scalmalloy® powder analysed (Spektrum 89)*

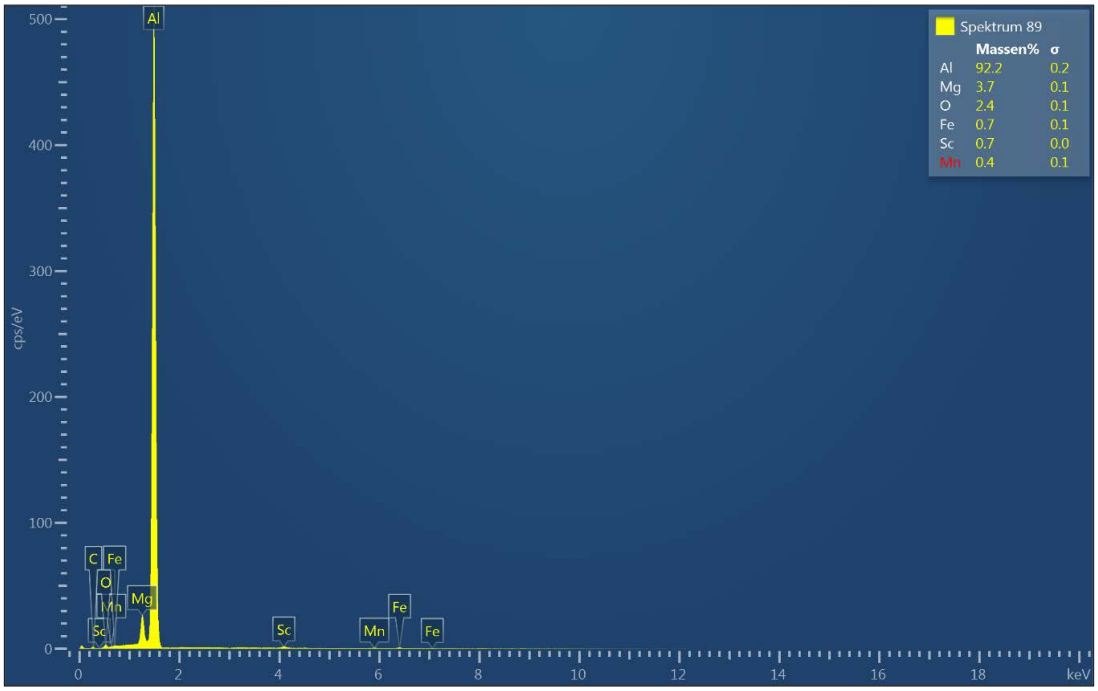

Figure 3-12 *EDS spectrum of Scalmalloy® powder analysed (Spektrum 90)*

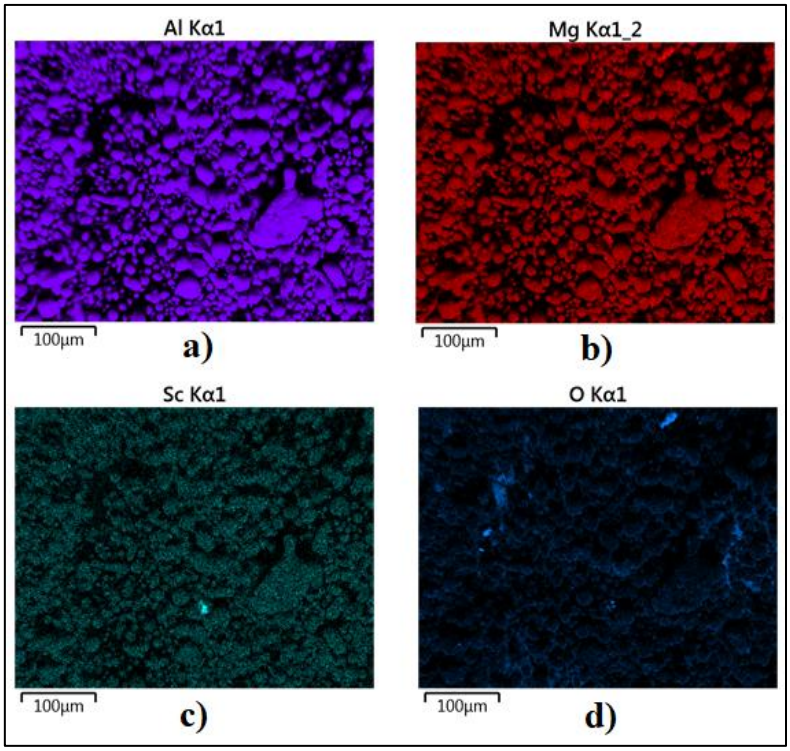

Figure 3-13: *Compositional distribution of Aluminium (a), Magnesium (b), Scandium (c) and Oxygen (d)*

As can be seen from the different EDS spectra obtained on the three localized regions of powder and from the images acquired following the mapping (Figure 3-13), the oxygen content in the powder remains significant.

Figure 3-14 shows an image obtained using the high magnifications allowed by the SEM. In particular, from this image it is possible to evaluate the irregular morphology of the Scalmalloy® powder and compare it with the AlSi10Mg powder (Figure 3-3). The particles of the latter have a much more circular shape. Moreover, noting the metric scale, it is easy to observe how Scalmalloy® particles have almost lower dimensions if compared with those of AlSi10Mg.

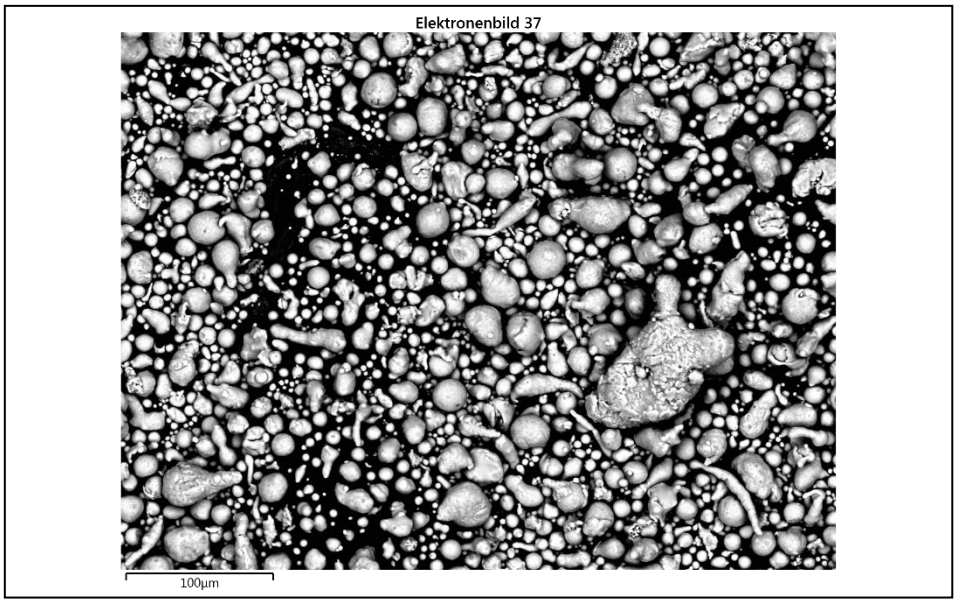

Figure 3-14: *SEM image of Scalmalloy® (higher magnification)*

4. Specific heat capacity

The fourth chapter describes the entire procedure necessary to calculate the specific heat, starting from the experimental heat flow curves. Great importance is given in this chapter both to the implementation of symmetry correction, by means of the STARe software, and to the determination of the effective mass of the sample by means of DSC analyses.

4.1. Heat capacity determination

It has been widely discussed above that "Powder Bed Fusion" techniques allow the production of a wide range of components, even those with very complex geometric characteristics. However, the efficient use of this technique requires an accurate analysis of different operating parameters. A parameter of considerable importance, for which it is necessary to make an accurate assessment in the modeling phase, is the specific heat capacity of the material.

According to Equation 2.5, the heat flow to which the sample is subjected is defined by the sum of the heat loss function Φ_1 and the product of the sample mass m, its specific heat capacity c_p and the scanning rate β. By using one of the two correction procedures (Section 2.1.2.8), it is possible to exclude the heat flow contribution relative Φ_1 through a simple subtraction. The result is a simplified equation:

$$c_p = \frac{\Phi}{m \cdot \beta} \quad (4.1)$$

As can be seen from Equation 4.1, the specific heat of the material can be easily calculated from this ratio. However, there is another variable that is not known in advance: the mass of the sample (m). Since the samples used for the different analyses are hold micrometric dimensions, a simple gravimetric measurement is unsuitable for obtaining this mass value. It is therefore necessary to carry out specific thermal analyses on the same material and utilise Equation 2.4.

The calculations necessary were carried out using the graphical analysis capabilities of STARe Software and the data obtained from the experiments performed with Netzsch DSC204 F1 Phönix and METTER-TOLEDO FlashDSC 2+.

4.1.1. Heat flow calculation

The thermal analyses performed using Flash Differential Scanning Calorimetry have allowed obtaining the heat flow trend of the sample during heating and cooling. Figure 4-1 shows the results of the thermal analysis, performed with METTER-TOLEDO FlashDSC 2+, on a particle of Scalamlloy® powder. These curves represent the heat flow (Φ) for heating and cooling. The appearance of the melting peak, during the heating phase, and of a recrystallization peak, after cooling, can be observed.

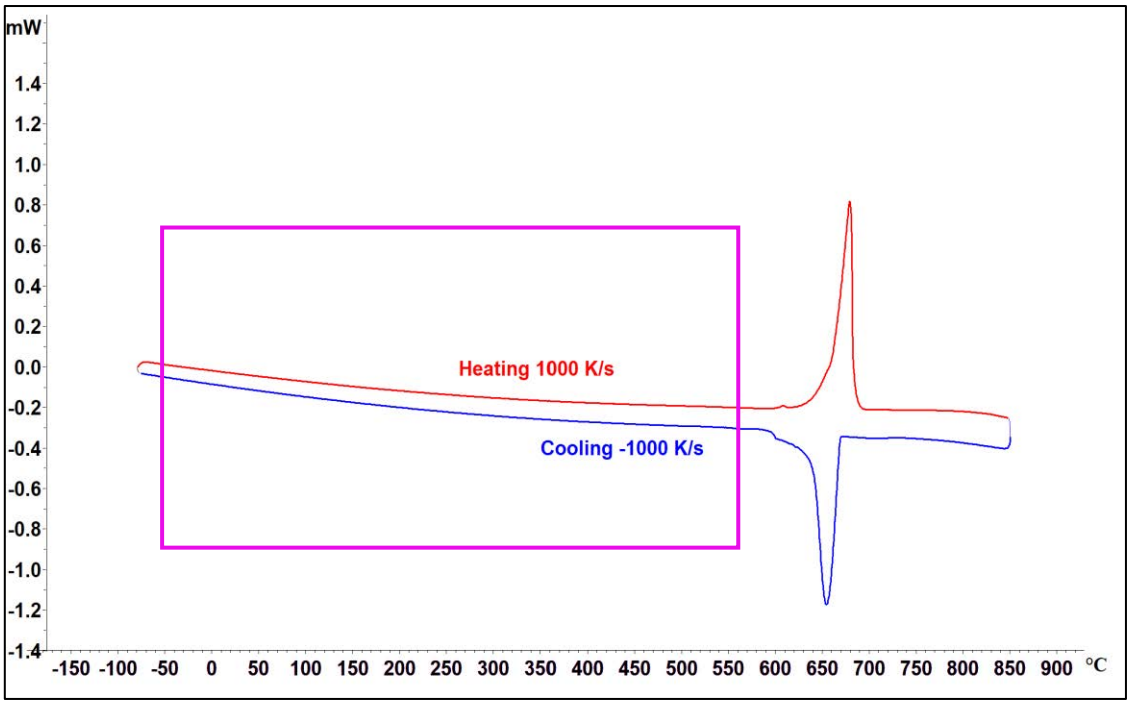

Figure 4-1: *Heat flow curve of Scalmalloy® for a heating rate of 1000 K/s and cooling rate of -1000 K/s*

As described in § 2.1, for these measurements it is necessary to implement a suitable temperature program in the relative software, according to the objectives of the analysis and the type of material being analyzed. For the purpose of this project, thermal conditioning programs consisting of several temperature segments were used, setting a

temperature range between -80°C and 850°C (higher than the melting point of aluminum alloys studied). An example of a temperature program is shown in Figure 4-2.

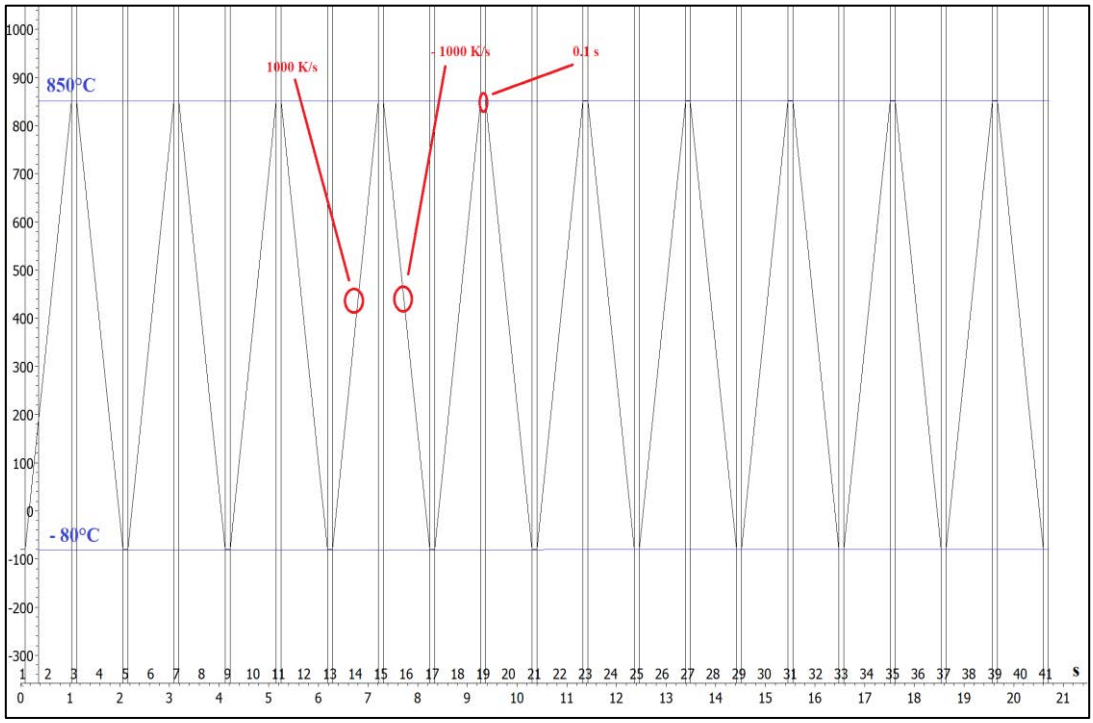

Figure 4-2: *Temperature program with 11 steps (ΔT = -80°C ─ 850 °C, Heating = 1000 K/s, Cooling = -1000 K/s)*

All the analyses were aimed at studying the development of the specific heat, as a function of the temperature, which characterized the metallic sample during its solid phase. From a graphical point of view, the determination of the heat flow was conducted by evaluating the portion of the experimental curve lower than the melting point of the sample itself. Afterward, the calculation of the heat loss function (Φ_1) was performed, implementing the *symmetry correction*. As described in Section 2.1.2.8, this method involves the calculation of the average heat flow between heating and cooling (dashed curve in Figure 4-3). Subtracting the average value (heat loss function) from the total heat flow of the sample removes the contribution related to Φ_1, as shown in Figure 4-4.

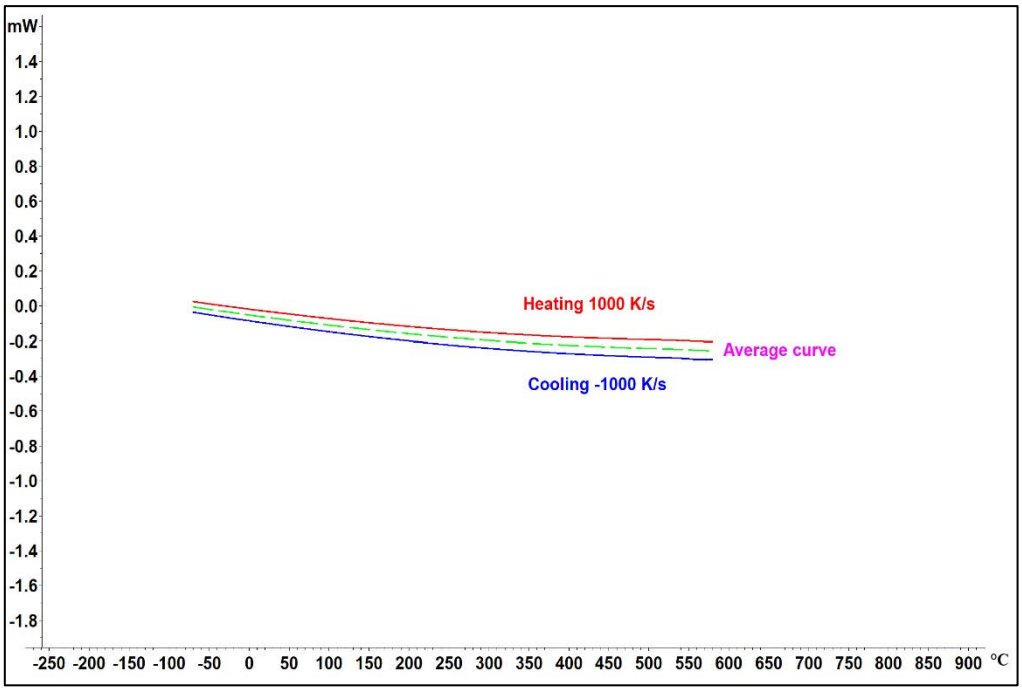

Figure 4-3: *Section of heat flow curve and average curve between heating and cooling*

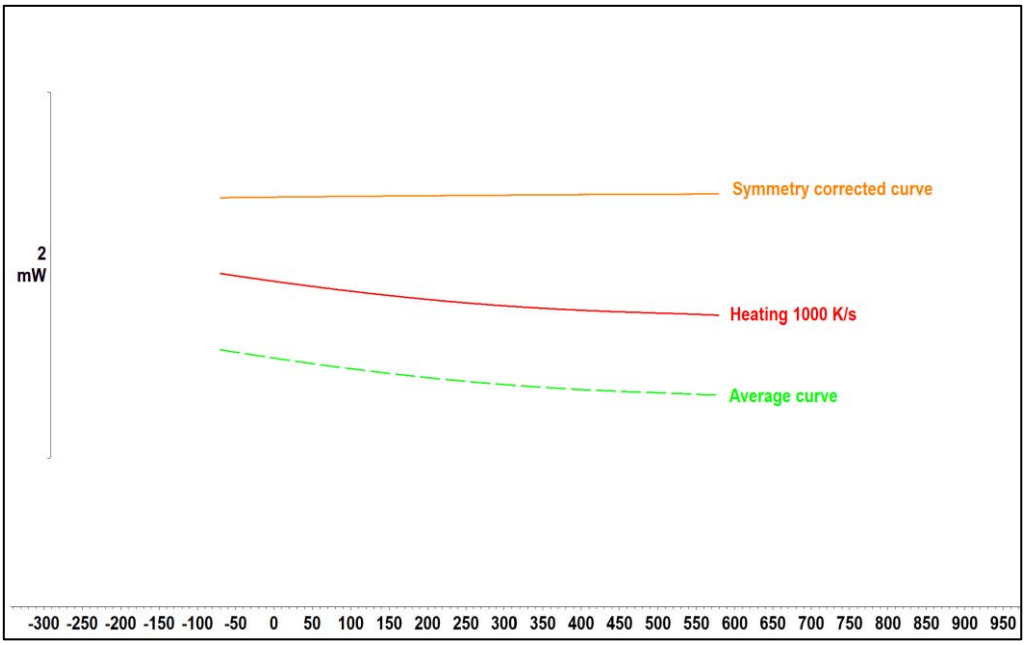

Figure 4-4: *Heat flow corrected curve obtained from the heating of the sample by symmetry correction*

4.1.2. Sample mass calculation

Previously, the complete correction procedure implemented for the overall evaluation of the heat flow has been described. However, the effective calculation of the specific heat capacity requires the knowledge of a further variable, namely the effective mass of the sample under analysis. According to Equation 2.4, the mass of the micrometric sample can be calculated as the ratio of the enthalpy of melting to the specific enthalpy of fusion of the material. From an experimental point of view, this parameter can be obtained using the following formula:

$$m = \frac{Enthalpy\ of\ melting\ from\ FDSC\ analysis}{Specific\ enthalpy\ of\ fusion\ from\ DSC\ analysis} \tag{4.2}$$

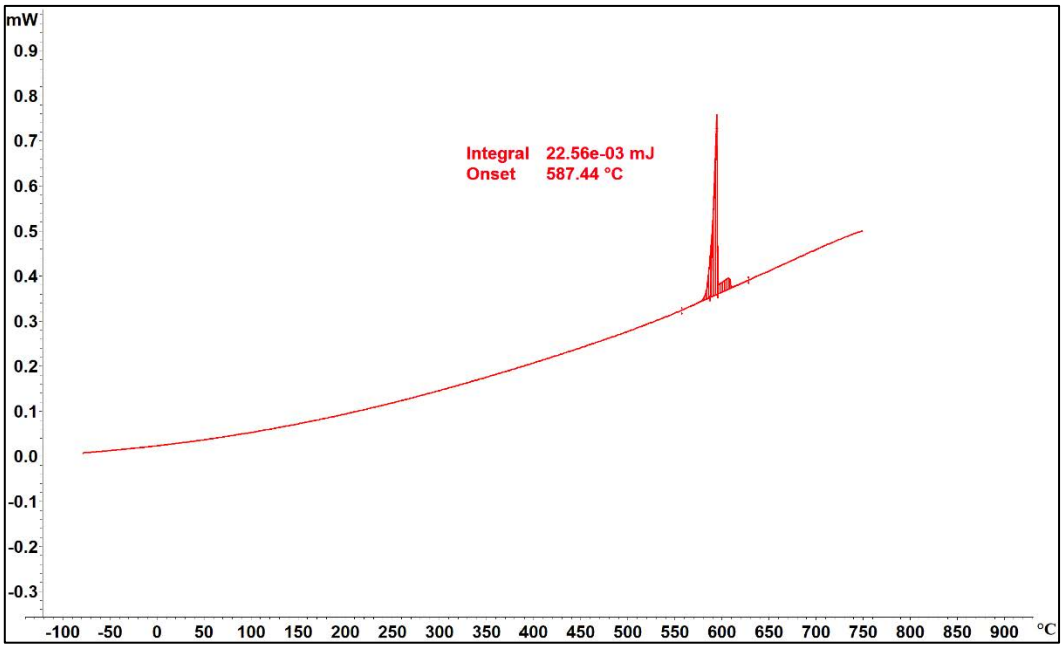

Figure 4-5: *Enthalpy of melting evaluation of AlSi10Mg sample (Heating = 100 K/s, Cooling = -100 K/s)*

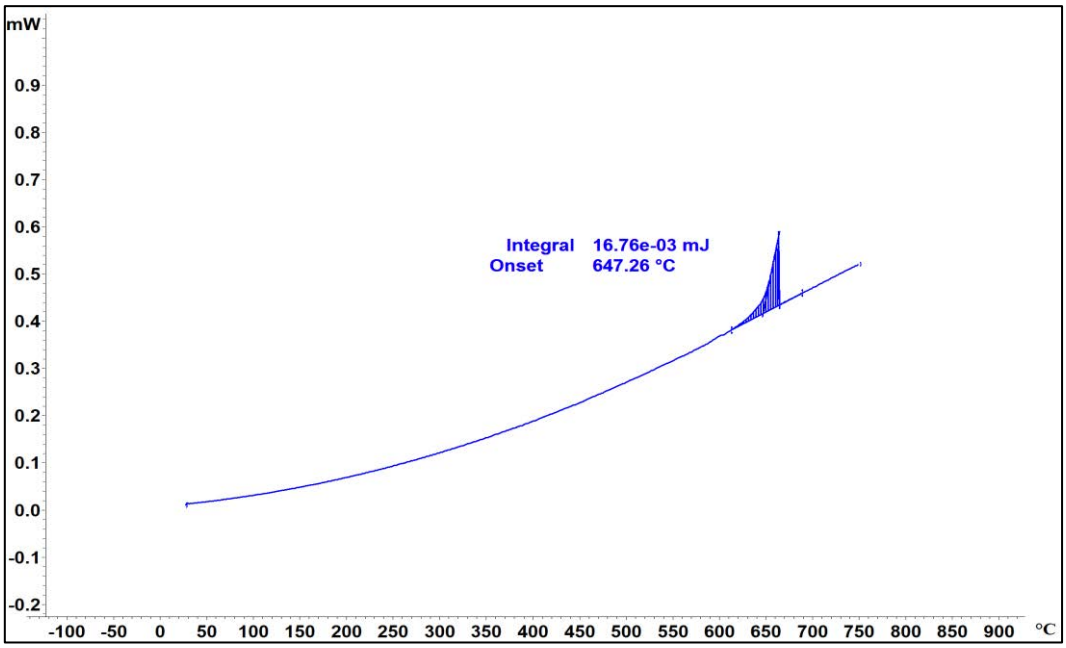

Figure 4-6: *Enthalpy of melting evaluation of Scalmalloy® sample (Heating = 100 K/s, Cooling = -100 K/s)*

The enthalpy of melting (energy of melting) is determined just by evaluating the integral of the melting peak from FDSC analysis curves, generally obtained from the pre-melting procedure. In Figures 4-5 and 4-6 the results obtained from this analysis are shown in terms of enthalpy of melting and melting temperature of the sample.

The second term of Equation 4.2 represents the specific heat of fusion, in J/g, of the tested material. To obtain this value, DSC analyses were carried out on the two types of powder using the Netzsch DSC204 F1 Phönix. This type of thermal analysis involves placing a portion of metal powder, weighed and compressed, into a crucible of alumina. The latter is carefully placed inside the analysis chamber along with a second empty crucible which is the reference. Both crucibles are subjected to the same temperature program and to an inert atmosphere, obtained by flushing argon into the chamber. For the DSC analyses, the correction procedure is performed by implementing the same thermal program, but with empty crucibles (*blank correction*). Also in this case the specific enthalpy of fusion is obtained by evaluating the integral of the melting peak of the curve.

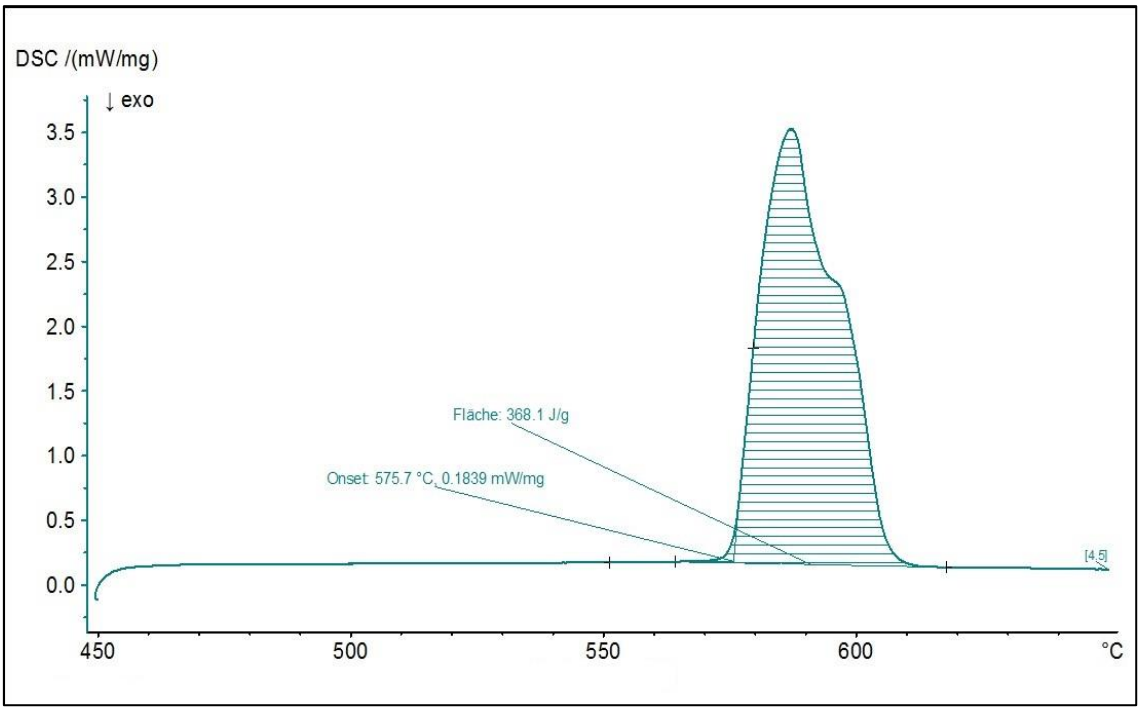

Figure 4-7: *Melting peak evaluation of DSC analysis on AlSi10Mg powder*

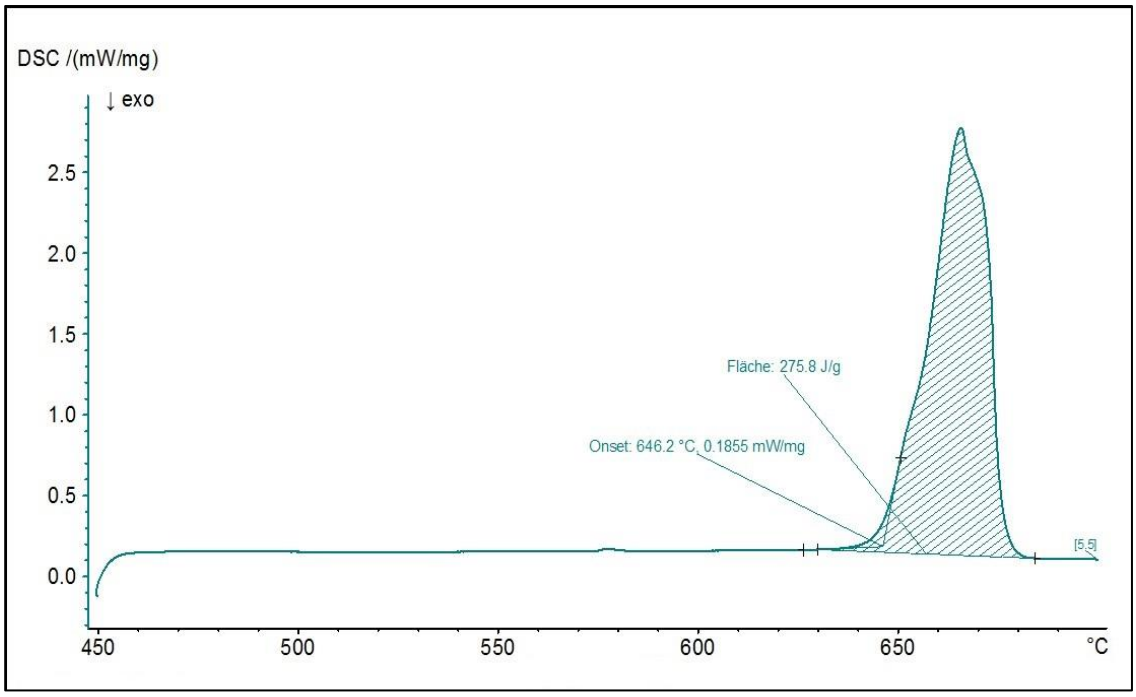

Figure 4-8: *Melting peak evaluation of DSC analysis on Scalmalloy® powder*

Through two thermal analyses it was therefore possible to determine the variables necessary for calculating the mass of the sample under analysis. The different values are summarized in Table 4.1.

Materials	**Sensor ID**	**Melting Temperature**	**ΔH_{melt} (FDSC)**	**ΔH_{melt} (DSC)**	**Sample Mass**
		[°C]	[J]	[J/g]	[µg]
AlSi10Mg	48671	575.7	2.22E-05	368.1	0.0584
Scalmalloy®	48670	646.2	1.68E-05	275.8	0.0604

Table 4.1: *Mass of samples*

5. Results

The purpose of the fifth and last chapter is to report the results obtained from the FDSC analysis conducted on the two metal powders. These results are then compared with the curves of a high-purity aluminium sample and with the data obtained from literary sources. Finally, from this comparison, it is possible to draw appropriate conclusions which allow statements on the efficacy of the characterization technique used for the study of specific heat.

5.1. Specific heat capacity results

Once the heat flow to which the sample is subjected has been determined in the FDSC analyses, and the actual mass of the sample has been calculated, the determination of the specific heat capacity of the material may be performed. This calculation is made by applying Equation 4.1 to the corrected curve. Figure 5-1 shows the variation of the value of the specific heat with the temperature, for a Scalmalloy® particle during the heating, without applying the correction procedure.

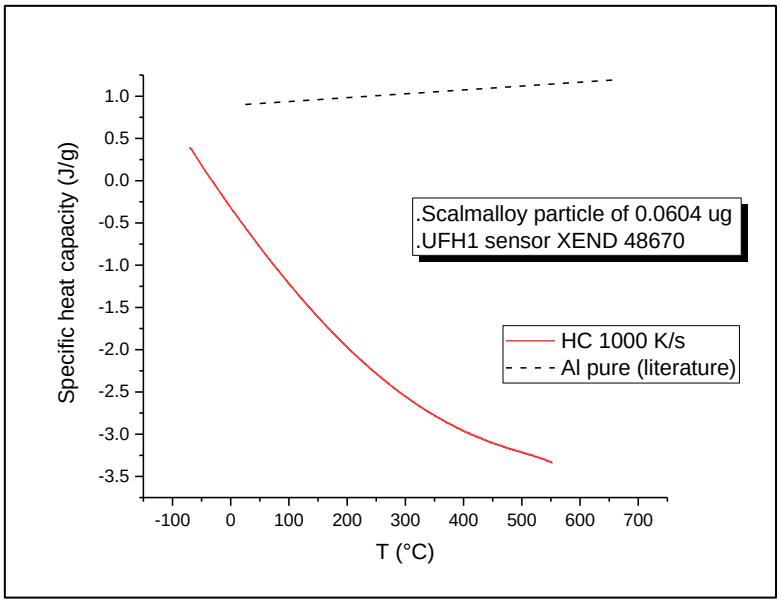

Figure 5-1: *Specific heat capacity trend of Scalmalloy®*

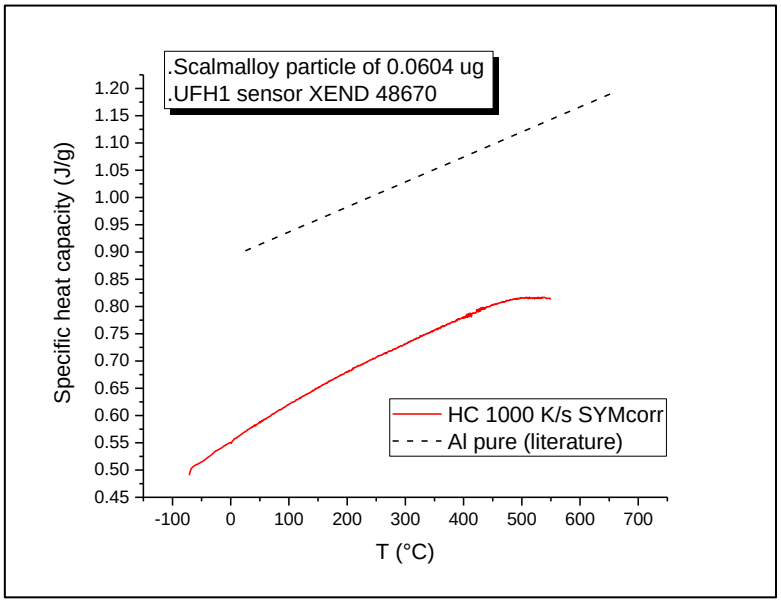

Figure 5-2: *Specific heat capacity trend of Scalmalloy®, obtained with symmetry correction*

In contrast, Figure 5-2 shows the results obtained using the symmetry correction procedure. As can be seen from the figures reported above, the values achieved by using or not the correction method are drastically different. This observation is remarkably underlined by the comparison with the data found in literature, in which the linearly increasing trend of the specific heat capacity of pure aluminium is reported. It is confirmed that the use of a specific correction procedure, aimed at neglecting the heat loss function, allows achieving more appreciable results and is more consistent with the theoretical values.

5.1.1. FDSC curves for different materials

The analytical procedures described in Chapter 4 were then applied in depth for AlSi10Mg and Scalmalloy® powders. The same sampling and analysis method were used for both materials. In particular, for each type of powder, specific thermal condition programs were implemented, varying the heating and cooling rates between 1000 and 30000 K/s, and using a flow of cold argon to cool the chamber (80 ml/min). In order to perform an accurate comparative analysis between the types of materials, it was decided during the project to carry out the same analysis on samples of pure aluminium. This comparison is essential given the relative closeness of the heat capacity values for

AlSi10Mg [47] and Scalmalloy [48] powders, obtained in previous studies, to the theoretical results for pure aluminium. In the latter case, the sample was prepared by sectioning a micrometric portion of a high-purity aluminium foil. Also for pure aluminium, the same calculations were carried out at the graphic and analytical level, necessary for the determining of the heat flow and the sample mass.

Materials	**Sensor ID**	**Melting Temperature**	**ΔH_{melt} (FDSC)**	**ΔH_{melt} (DSC)**	**Sample Mass**
		[°C]	[J]	[J/g]	[µg]
High-purity aluminim	48665	690	1.690E-05	388.1	0.0435

Table 5.1: *Mass of Aluminum high-purity*

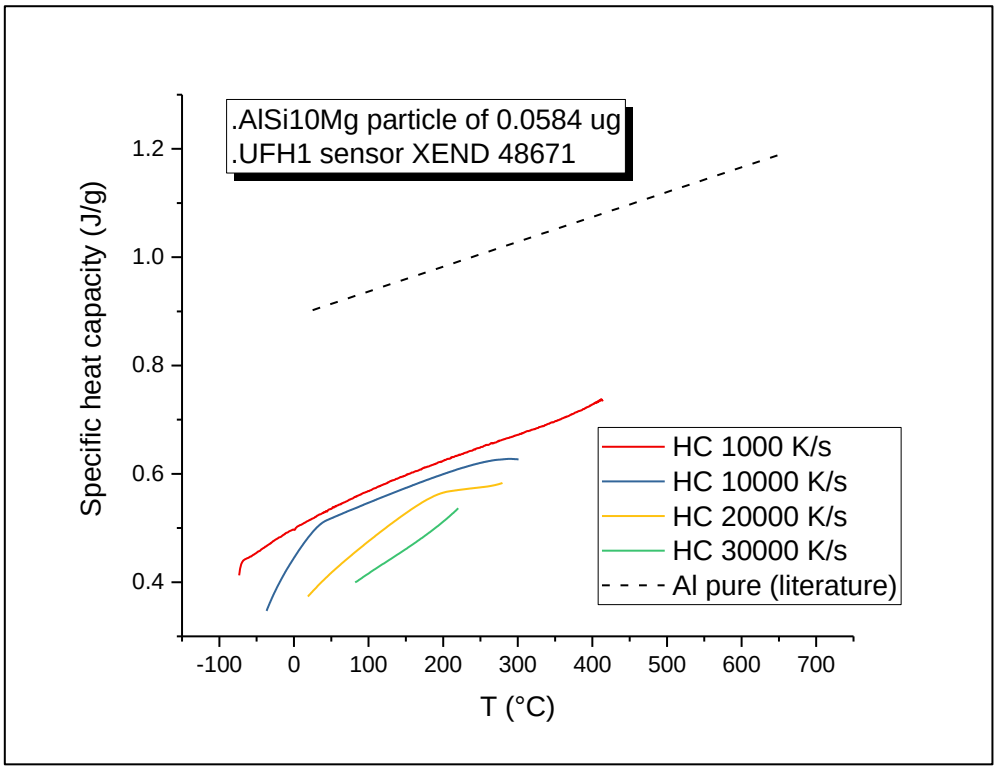

Figure 5-3: *Specific heat capacity trend of AlSi10Mg, for different scanning rates*

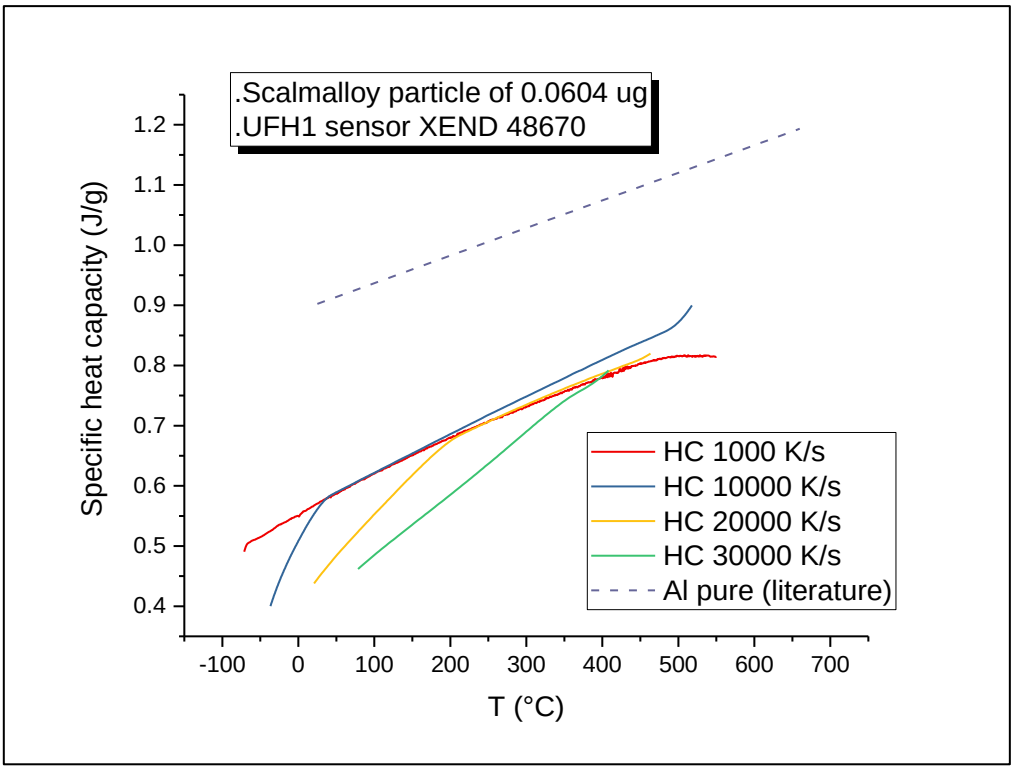

Figure 5-4: *Specific heat capacity trend of Scalmalloy®, for different scanning rates*

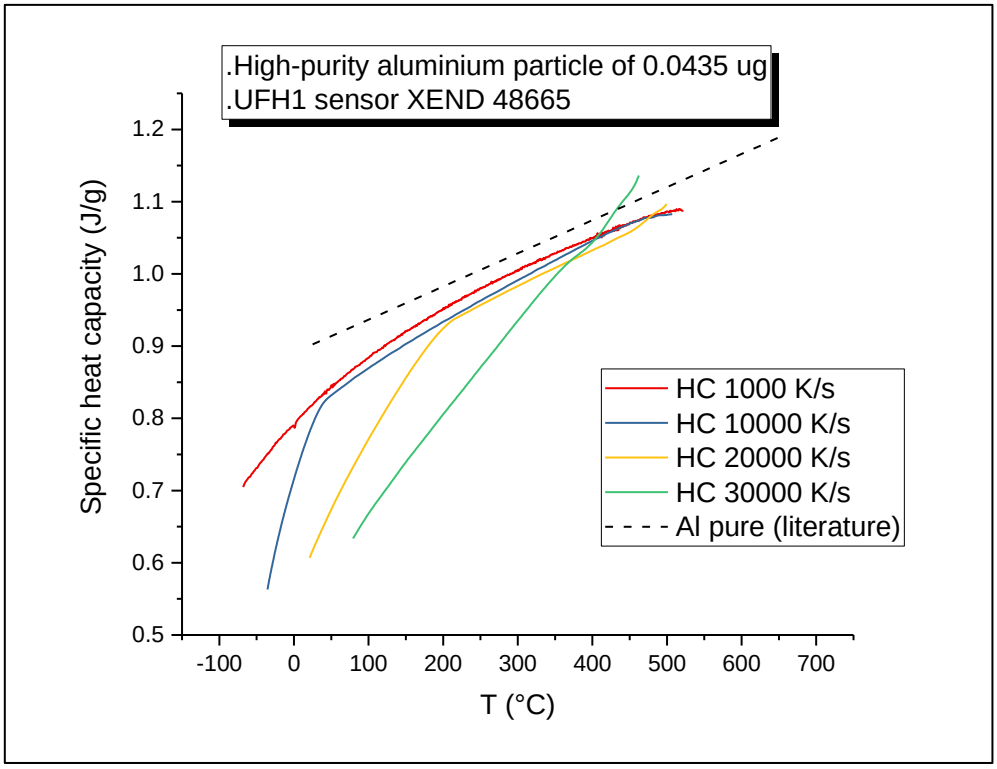

Figure 5-5: *Specific heat capacity trend of high-purity aluminium, for different scanning rates*

5.2. Issue relating to the sample characteristics

Figures 5-3, 5-4, and 5-5 reported above show the results obtained by means of FDSC analyses conducted on the different types of materials: AlSi10Mg, Scalmalloy® and high purity aluminium respectively. A first observation that can be made with regard to these graphs, concerns the trend of the value of the specific heat capacity. As can be seen, all the curves relating to the specific heat exhibit values that increase with temperature. Furthermore, this behaviour not only occurs for all three types of analysed materials but is also independent of the scanning rate set. This preliminary observation affirms how the use of the Fast Scanning Calorimetry obtains results in accordance with the different data in literature.

Although this technique of characterization is in keeping with the other more consolidated procedures, with regards to the general trend of the specific heat, more accurate analysis of the results reveals deviations from the theoretical reference value. As mentioned above, although the two aluminium alloys under study are very different from pure aluminium, in terms of composition and properties, the data reported in the literature show that the trends and values of the specific heat are very similar to those of pure metal (dashed line reported in the different figures). In particular, these differences can be more or less significant compared to the theoretical values, depending on both the type of material and the scanning rate used, and can be attributed to issues relating to the method of analysis.

5.2.1. Specific heat trend and thermal lag influence

As widely pointed out in previous chapters, this thesis project aims to evaluate the specific heat capacity of particular metal samples, subjecting them to a certain rate of analysis and varying the temperature in a range between -80°C and the melting point of the powder under analysis. It is for the latter reason that it was necessary to determine analytically not only the mass of the sample, necessary for the actual calculation of the specific heat through an appropriate correction procedure, but also the melting temperature of the metal. This value aids in analysis by limiting the dissection of the heat flow curves to a temperature range, in which the sample is present in the solid-state.

As described in Chapter 4, the melting temperature of a given sample was determined by the melting peak of the heat flow curve. From a purely theoretical point of view, the

temperature at which a given metal is melted is independent of the scanning rate at which this temperature is reached, and therefore all the curves shown in the various graphs should represent the values of specific heat up to the melting point of the metal. This condition does not seem to be present in the results obtained. Observe not the experimental curves, but their projection on the temperature axis. From the different graphs it can be observed how the temperature range in which representation of the specific heat occurs, decreases with the increase of the scanning rate. In some cases, the calculated melting point is not even reached, as can be seen from Figure 5-3, relative to the analyses carried out on AlSi10Mg (Temperature of melting = 575,7 °C). For the other two types of material this phenomenon is still present but is much less marked.

The reduction of the range of results, in the function of the set rate, is certainly related to the sectioning phase of the curve, performed during the procedure of calculation of the specific heat. The dissection of the curve, as shown in Figure 4-1, was performed starting after the initial interval of stabilization, up to the temperature for which there was the appearance of the melting/solidification peak. A change of the position of the peak, at lower temperature, or an increase in the initial interval, causes the reduction of this range. The main cause of this problem is the thermal lag related to the measuring instrument.

The thermal lag is a phenomenon that occurs in all instruments used for calorimetric analysis, because of the non-ideal thermal transfer that is established between the heating elements and the sample. However, the cause can be considered different depending on the instrument employed. In the case of a DSC device, the thermal lag between the controlled furnace temperature and the sample temperature is directly related to the crucible and the sample used. On the other hand, in Flash DSC instruments this problem is determined almost exclusively by the sample and its contact to the sensor. In particular, the thermal lag can cause a variation of the measured onset temperature (T_{on}) of the melting or solidification peak, as the scanning rate varies. As reported in *Fast Scanning Calorimetry* [39], the dependence of thermal lag (τ_{lag}) on the scanning rate (β) can be described by the following equation:

$$T_{on} = T_{on,0} + \tau_{lag} \cdot \beta \quad (5.1)$$

Where $T_{on,0}$ is the onset temperature extrapolated to a scanning rate of 0 K/s.

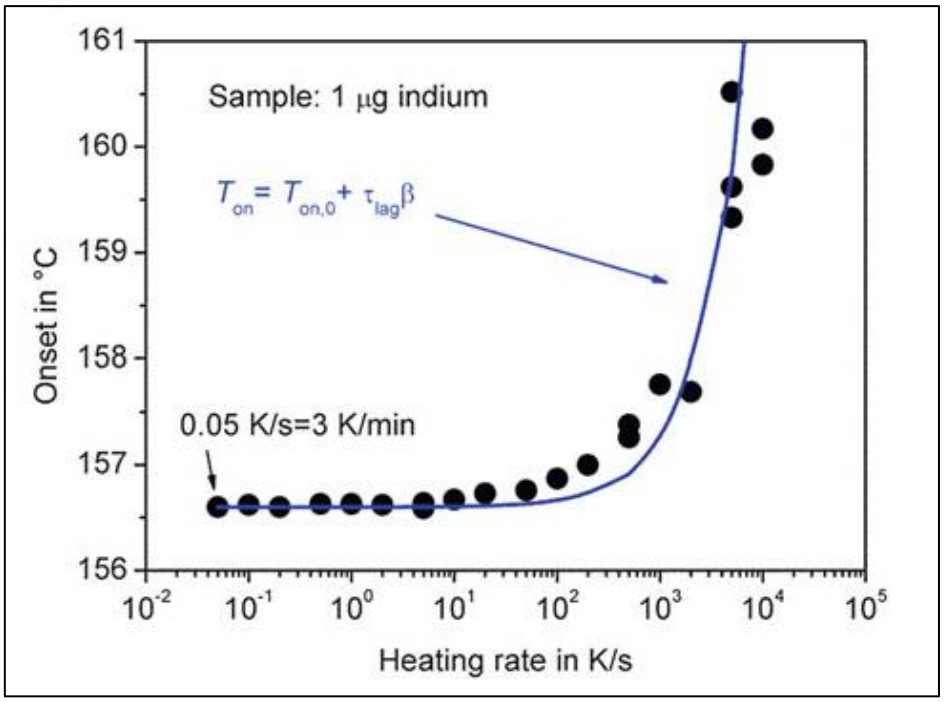

Figure 5-6: *Onset temperature of the melting peak of indium, as a function of the heating rate [39]*

Figure 5-6 shows the onset temperature of the melting peak of an indium sample, as the heating rate varies. As it can be seen, the phenomenon of thermal lag is very limited for lower rates, about 10^2 K/s, and then undergoes a rapid increase for values of higher rates, as shown from the fitting curve. It is for this reason that the calculation of both the sample mass, and that of its melting temperature, was performed on the heat flow curve obtained at 100 K/s, so as to allow to neglect the effect of thermal lag.

As mentioned above, this phenomenon has also been observed in the experimental curves obtained during the development of this project. In particular, Figure 5-7 shows the different heat flow curves for the analyses carried out on Scalmalloy® powder obtained during the heating and cooling phases. As can be seen by comparing the different curves, with the same sample mass there is an increase of the absolute value of the measured heat flow as the scanning rate increases (since more power is needed). Due to the thermal lag of the instrument, the increase in the programmed rate also causes not only the displacement of the melting and solidification peak, but also their progressive enlargement.

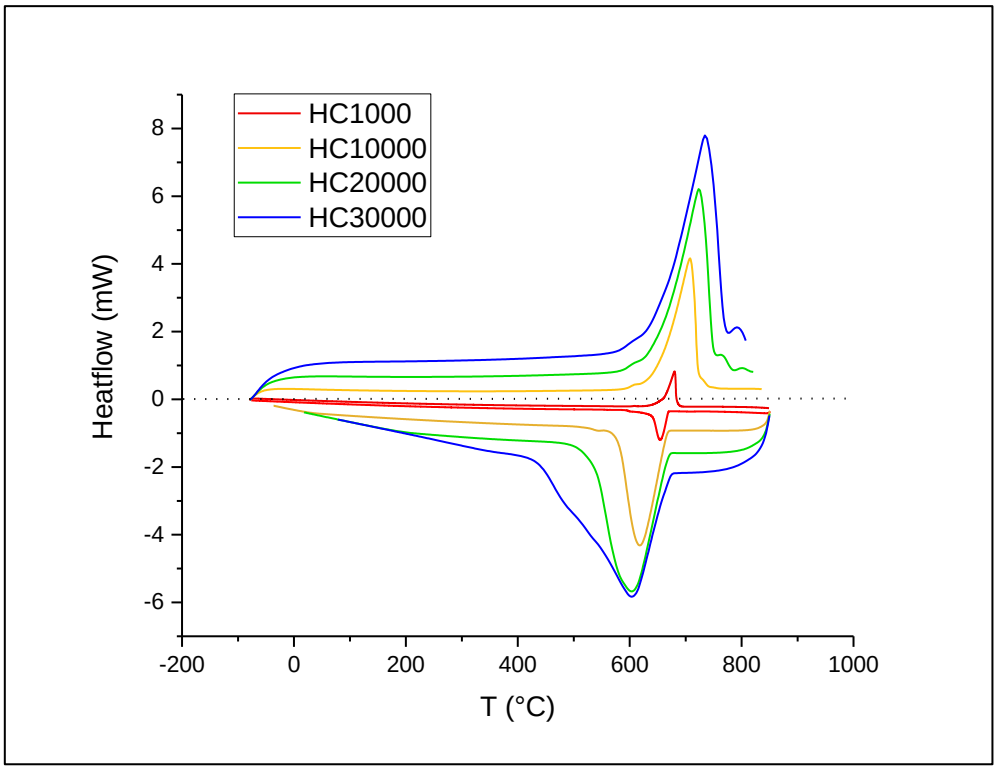

Figure 5-7: *Heat flow curves at different scanning rates*

Also worthy of note is the impact of the initial thermal stabilization on the measured heat flow. This phenomenon is recorded in the initial temperature ranges, causing a perturbation of the different curves. In particular, from Figure 5-7 and 5-8, it can be seen how this interval tends to increase as a function of the set rate, is strongly intensified for higher rates, and is therefore attributable to the thermal lag of the measuring instrument.

The increase of the stabilization interval, added to the variation of the position and shape of the melting and solidification peaks, according to the rate, make the thermal lag the main cause of the effective reduction of the range of the useful results. From Figure 5-8 it is possible to see the progressive decrease of the data interval on which to implement the correction procedure. For some scanning rates, the thermal lag not only reduces the set of measured values but also produces curves with a slope drastically different from the reference curve. Looking more in detail at the trend of the theoretical curve, with that of the measured curves, it can be observed how the slopes are conforming only after a point of discontinuity (Figure 5-9), positioned at a given temperature. By increasing the scanning rate, this point tends to move towards higher temperature due to the increasing of the thermal stabilization range, reducing the portion of the curve with a more conforming slope.

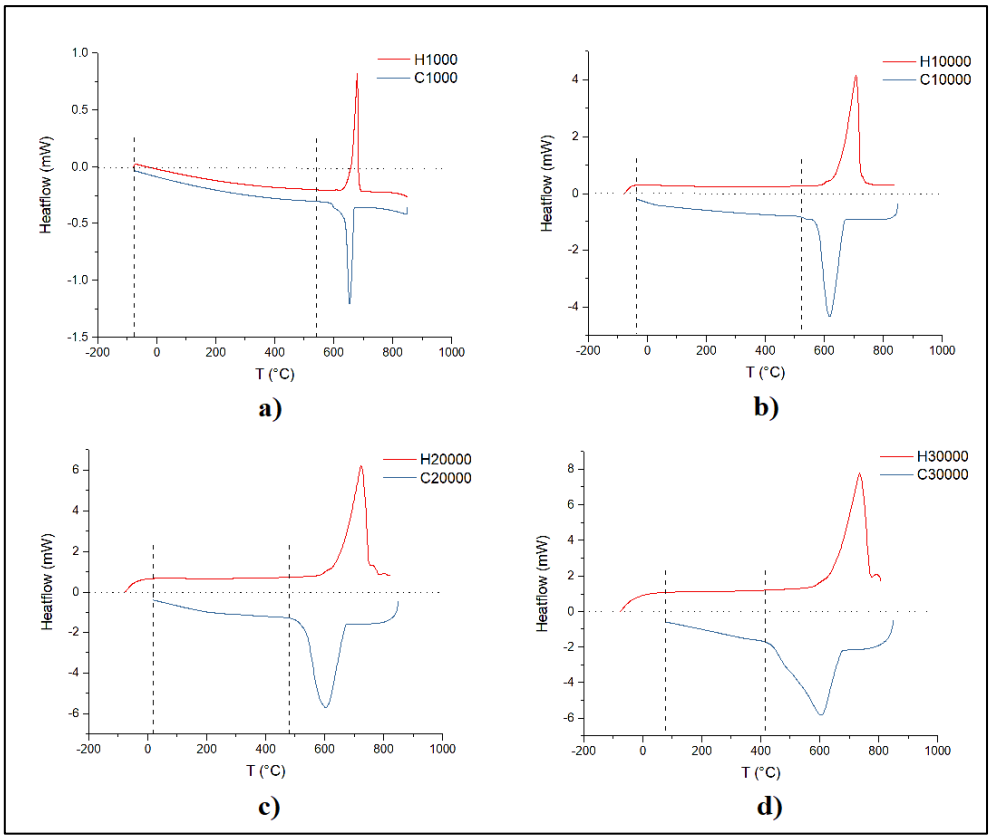

Figure 5-8: *Measuring range determined for different scanning rates*

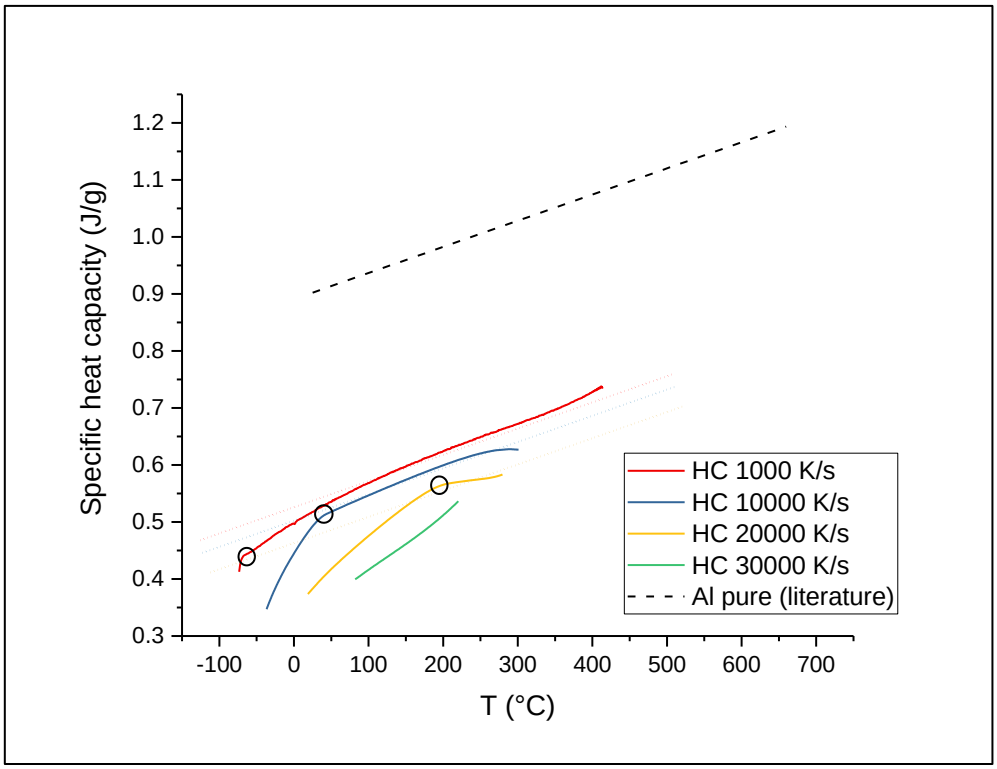

Figure 5-9: *Change of the discontinuity point with the scanning rate, for AlSi10Mg*

5.2.1.1. Causes of thermal lag

Previously it has been pointed out that, despite the different composition, the specific heat present in literature for the two types of aluminium alloys, is very similar to that of unalloyed aluminium. This equality should refer not only to the absolute value expressed by this property but also by its trend as it changes with the temperature. Theoretically the variation of the specific heat can be indicated according to a relationship of the type:

$$c_p(T) = A + B \cdot T \quad (5.2)$$

where A and B are two physical constants. However, it has already been discussed how the experimental curves, obtained from FDSC analyses, generally satisfy this relationship only in certain temperature ranges, depending on the scanning rate used.

As discussed in detail in the previous section, this behaviour is essentially associated with the thermal lag characteristic of the measuring instrument, a problem which is almost exclusively associated with the thermal contact between the analysis sensor and the sample. There may be various reasons for a decline in thermal contact, such as the morphology of the sample. It should be remembered that the aluminium alloy samples employed are powder particles, generally spherical in shape and microscopic in size. Although thermal melting programs were implemented before the different measurements in order to improve the sample contact, the high heating and cooling rates imposed may cause a partial detachment of the sample. Another factor that could influence the thermal contact of the sample, is also its composition, and in particular the percentage of bound oxygen. From the compositional analyses reported in Chapter 3, it can be observed that for both Scalmalloy® and AlSi10Mg powder, the percentage of oxygen is significant (greater than 5%). This element can easily bind with oxide-forming metal, including aluminium, and lead to the formation of surface layer of oxide. Given the insulating nature of aluminium oxide, its surface presence could certainly cause a decrease in thermal contact.

5.2.2. Experimental absolute values

Among the three types of analysed materials, from the data reported in Section 5.1 it can be noted that the results most in line with the reference data are those relating to high-purity aluminium. This condition can be underlined both in terms of specific heat trend and absolute value. Regarding the differences expressed between the absolute values of the experimental and theoretical data, although the specific heats of the two alloys can be considered very similar to those of pure aluminium, the different composition of these alloys lead to a differentiation of this property, with respect to unalloyed metal. In Chapter 1 it was considered how the composition of a given metal significantly influences the value of the specific heat according to the Neumann-Kopp's rule. Equation 1.4 can be used to explain the differences in absolute value found for AlSi10Mg, with respect to pure aluminium. In particular, the lowering of the global specific heat capacity of this alloy can be attributed to the high percentage of silicon present, about 10%. This element is characterized by a much lower specific heat (0,7 J/g) than that of pure aluminium (0,88 J/g). Because of this difference, there is an overall decrease in the linear combination expressed by Neumann-Kopp's rule.

Although the observed reduction finds a theoretical confirmation, this lowering of the obtained values is too severe. This inconsistency is further confirmed by analysing the experimental curves of the other two samples. Low specific heat values were also found for Scalmalloy® powder. However, if in the case of AlSi10Mg this phenomenon can be partly explained by the presence of silicon in the overall composition, for this second type of powder the causes could be different. As described in Chapter 3, the Scalmalloy® powder analysed shows a magnesium content of about 4.5%, which is characterized by a specific heat much higher than aluminium. According to Equation 1.4, in this case, higher experimental values should have been obtained than both high-purity aluminium and those searched in the literature.

An underestimation in the experimental results was also obtained for high-purity aluminium. In this case, however, this irregularity is less marked than for the two alloys. Most likely the better consistency between the theoretical and experimental values may be due to the different morphology of the sample. Unlike the two aluminium alloys, for which the analyses were carried out on powder particles, a small fragment of metal foil was used for high-purity aluminium. The use of a foil favours homogeneous heating of the sample and therefore better reproducibility in the measuring instrument. The greater

thickness of the metal powders could lead to temperature gradients within the sample. It should also be noted that foil's flat morphology increases the thermal contact with the sensor, making the trend as the temperature changes more in line with the theoretical data.

An additional source of inconsistencies from the reference values, may be the preliminary calculation of the sample mass. As described in Chapter 4, the mass of the metallic sample was determined through the integration of the melting peak, relative to the different samples used. Given the morphological and composition characteristics, powder particles analysed are characterized by a non-optimal thermal contact, resulting in inaccurate melting peaks. The subsequent integration can generate overestimations of the relative masses.

5.3. Criticality of analysis

It has been concluded that the characteristics of the sample, both in terms of composition and morphology, can be the cause of the differences that distinguish the experimental data from those sought in the literature. Nevertheless, the inconsistences observed for all the samples analysed are not only attributable to the sample itself, but also to the measurement technique and the analysis procedure.

5.3.1. MultiSTAR UFH1 sensor

In the previous sections of this chapter, underestimates in the results obtained from FDSC analyses have been highlighted. In some case, these inconsistencies are markedly severe, as for AlSi10Mg and Scalmalloy® powders, while for the high-purity aluminium sample the difference with respect to the reference values appears quite contained. However, it is thanks to differences found in the latter case, that it was possible to identify the potential cause of this problem in the measuring instrument. From the comparison between the experimental and reference curves, it is clear that the results obtained for high-purity aluminium are the most encouraging, given a global trend almost in line with that achieved by the data in the literature, and closeness between the different values. Surely this behaviour can be attributed to the use of a material similar to pure aluminium, represented by the theoretical data. However, there is still an underestimation of the specific heat, so much so as to consider the instrument of characterization as one of the possible causes, and no longer only the sample characteristics.

A MultiSTAR UFH1 sensor was used to carry out the necessary measurements. As extensively described in Chapter 2, it is a non-adiabatic chip calorimeter based on MEMS chip, consisting of a heater and a thermometer. With this sensor, it was possible to conduct measurements in wide heating and cooling range, beyond the maximum scanning rate limit of the conventional DSC. High heating rates can be achieved due to the low heat capacity of the measuring system, while the rapid cooling is permitted by the non-adiabatic conditions established inside the analysis chamber through the injection of cooling gas. For the various measurements is was decided to use an argon flow of 80 ml/min. Both the type of gas and its flow rate into the chamber of are fundamental parameters controlling the systems cooling. Depending on the type of gas, the thermal resistance between the calorimeter and the surrounding environment varies, leading to a

variation in the cooling rate. In particular, as the thermal conductivity of the gas increases, there is an increment in the cooling rate, due to reduction of the thermal resistance (Equation 2.2). According to Schick et al. [39], the gas flow must be set to a value higher than 50 ml/min, both to allow a homogeneous distribution of the gas around the sensor, and to avoid oxygen contamination.

It is easy to understand that if the heating phase of the sensor is easier to manage, by varying the electrical power to be supplied to the heater from the terminal, then the cooling phase is more complex. The cooling of the system can be done by varying the gas flow, keeping it above certain limits, or by varying the type of gas to be used.

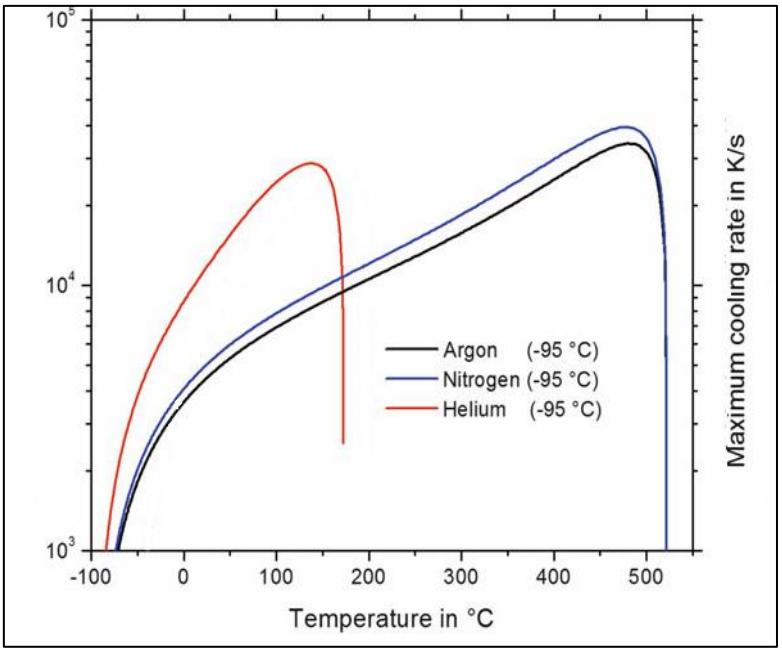

Figure 5-10: *Maximum cooling rates for He, N_2 and Ar. The ready temperature is set to -95°C [39].*

Figure 5-10 shows the maximum cooling rates achievable, depending on the types of gas used (He, N_2 and Ar). In the case of argon, it can be observed that the maximum possible cooling rate is about 20,000 K/s, well below the maximum scanning rate of analysis (30,000 K/s), and only for a narrow temperature range. For lower temperatures, even very low maximum cooling rates can be recorded.

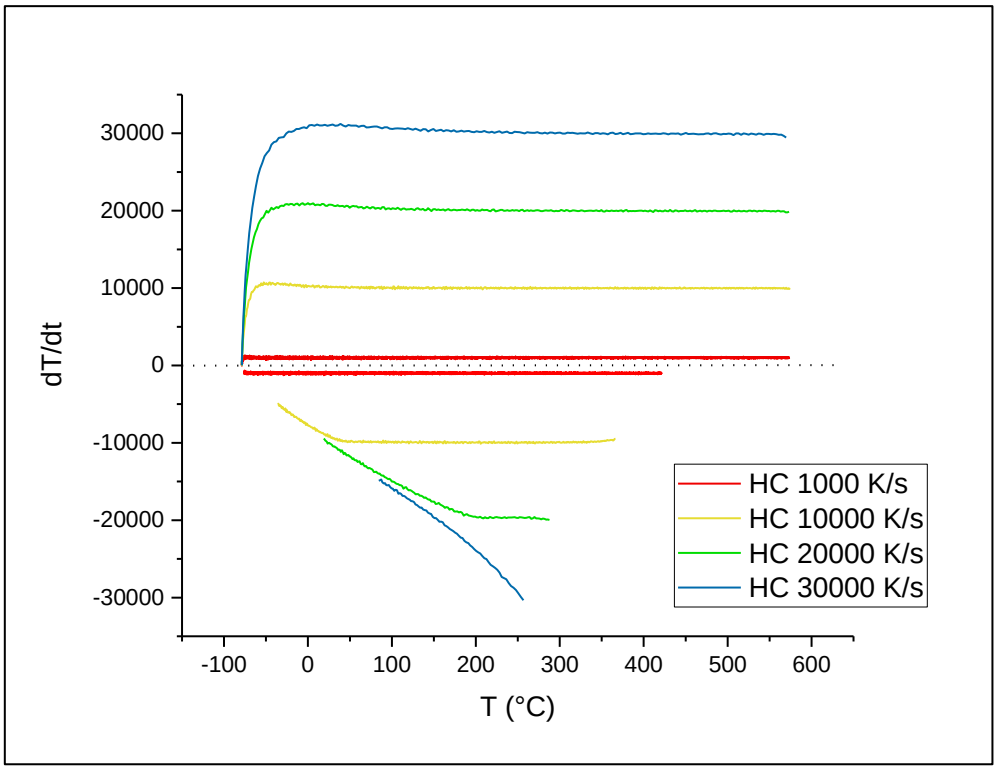

Figure 5-11: *Maximum scanning rates for AlSi10Mg*

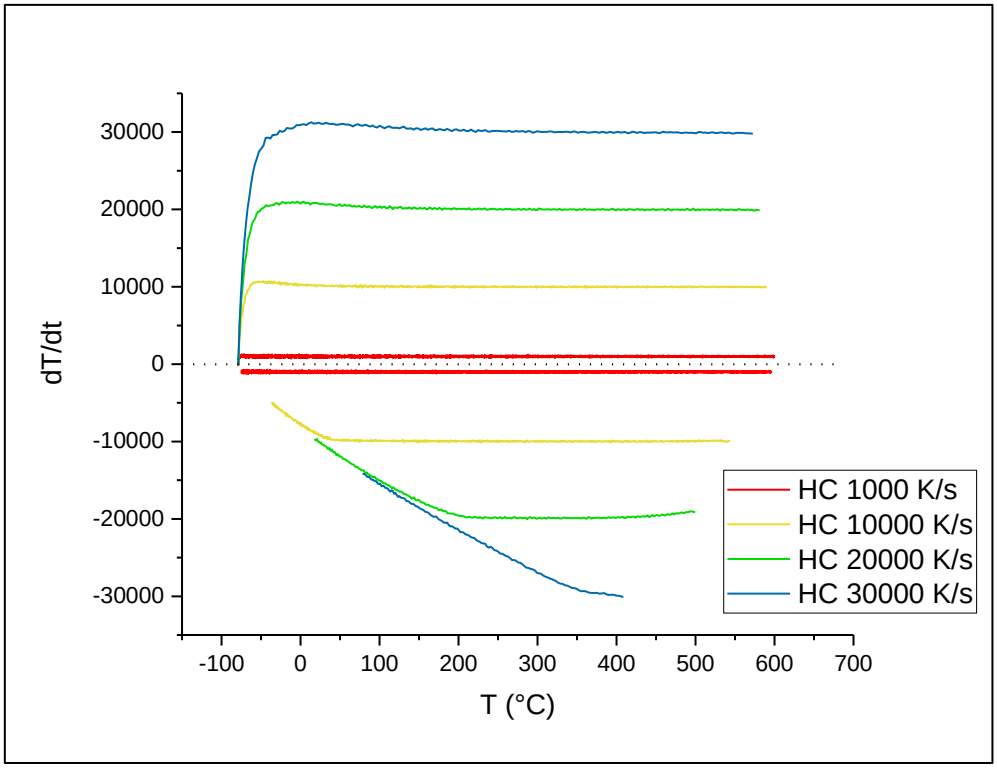

Figure 5-12: *Maximum scanning rates for Scalmalloy®*

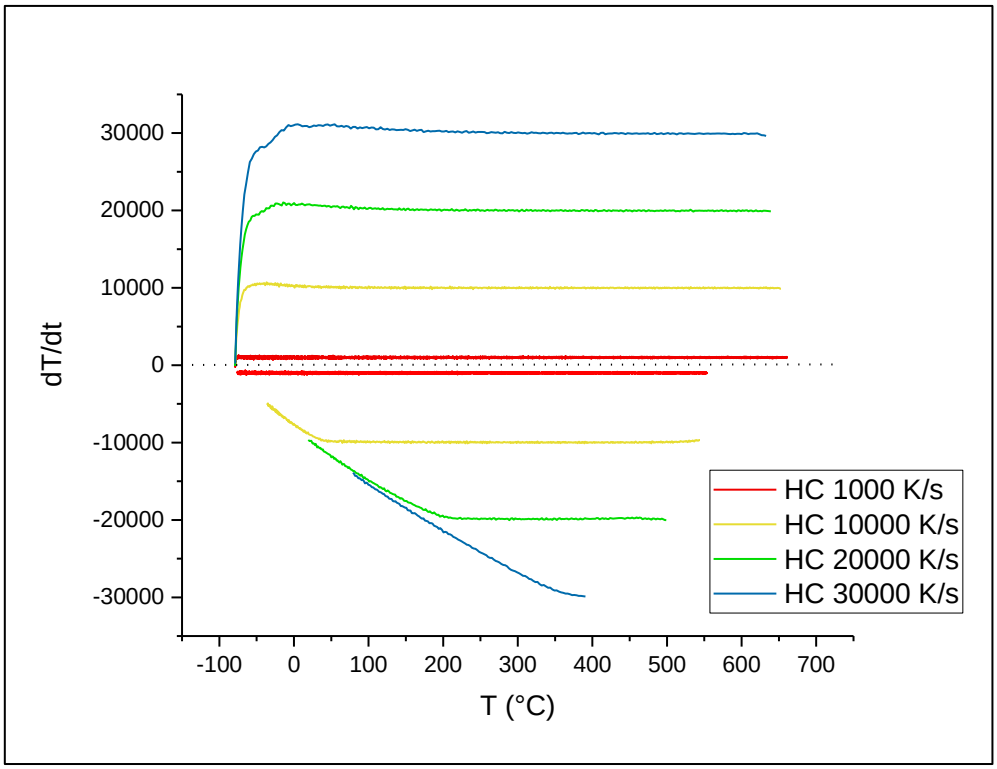

Figure 5-13: *Maximum scanning rates for high-purity aluminium*

This behaviour, registered during the cooling phase of the sample, represents one of the main causes of the underestimation of the experimental results. During the sample heating phase, the set scanning rate can be considered uniform throughout the analysed temperature range, however this behaviour does not occur during the cooling, therefore causing a non-symmetry condition between the two thermal steps. As shown in Figures 5-11, 5-12 and 5-13, this condition can be easily detected through the calculation of the derivates, related to the different scanning rates. The non-symmetry between the heating and cooling phase was observed for all three types of materials analysed, and with a variable intensity depending on the scanning rate. At 1000 K/s, an optimal symmetry between the two thermal steps is observed and for this reason, the underestimation relative to this rate can be attributed exclusively to the characteristics of the sample itself. The actual underestimation of the experimental specific heat values, can derive from the symmetry correction procedure, is mathematically demonstrated.

As described in Chapter 2, the symmetry correction can be used to determine the heat loss function by the average between the heating and cooling heat flow (Equation 2.7 and 2.8). However, this procedure results to be efficient for the objective researched only if a

perfect symmetry between the two phases is provided, and therefore that the heating and cooling rates are equal, in absolute value, throughout the thermal range of analysis ($\beta_h = \beta_c$). However, as previously observed, this symmetry is maintained only for certain temperature ranges, the broadness of which depends on the scanning rate. In general, it can be noted that the symmetry between heating and cooling, above a certain threshold scanning rate, decreases as the set rate increases.

Consider a condition of asymmetry between the heating and cooling steps, within a given temperature range. This condition implies that the two scanning rates will be different, for a certain temperature within this range: $\beta_h \neq \beta_c$.

$$\Phi_{avg} = \frac{\left(m \cdot c_p \cdot \beta_h + \Phi_1\right) + \left(m \cdot c_p \cdot (-\beta_c) + \Phi_1\right)}{2} \quad (5.3)$$

$$\Phi_{avg} = \frac{2\Phi_1 + m \cdot c_p \cdot (\beta_h - \beta_c)}{2} > \Phi_1 \quad (5.4)$$

For this reason, the average heat flow will not be equal to the heat loss function, but a higher value will be obtained, according to Equation 5.4. The subsequent subtraction of the average value from the total heat flow will therefore lead to a lower value ($\Phi^{\#}$) than that theoretically expected in the case of perfect symmetry between the two phases (Φ).

$$\Phi^{\#} < \Phi \quad (5.5)$$

$$c_p = \frac{\Phi^{\#}}{m \cdot \beta_h} \quad (5.6)$$

Equation 5.6 shows how this reduction of the detected heat flow leads an overall decrease of the specific heat.

5.3.2. Slow-rate correction

For the overall evaluation of the specific heat values of the project's selected materials, it was decided to implement a symmetric correction procedure in order to neglect the heat loss function present in the measured heat flows. However, symmetry correction is not

the only correction procedure possible, and may not be the most optimal for the objectives sought. Thanks to the work carried out by Quick et al. [41], today the evaluations of the specific heat, obtained by FDSC analyses, can also be performed by the application of a second correction procedure: the *slow-rate correction.*

As described in Chapter 2, the two types of procedure can be considered equivalent, since both aim to eliminate the heat loss function. However, the two theoretical aspects are substantially different. The symmetry correction calculates the heat loss function from the average between the heat flow of heating and cooling, whereas with the slow-rate correction Φ_1 is evaluated using a low scanning rate (1 K/s), as reported in Equation 2.6. Once Φ_1 is identified, it is subtracted from the measured heat flow, as shown in Figure 5-14, and the specific heat can be calculated using the same method described for symmetry correction.

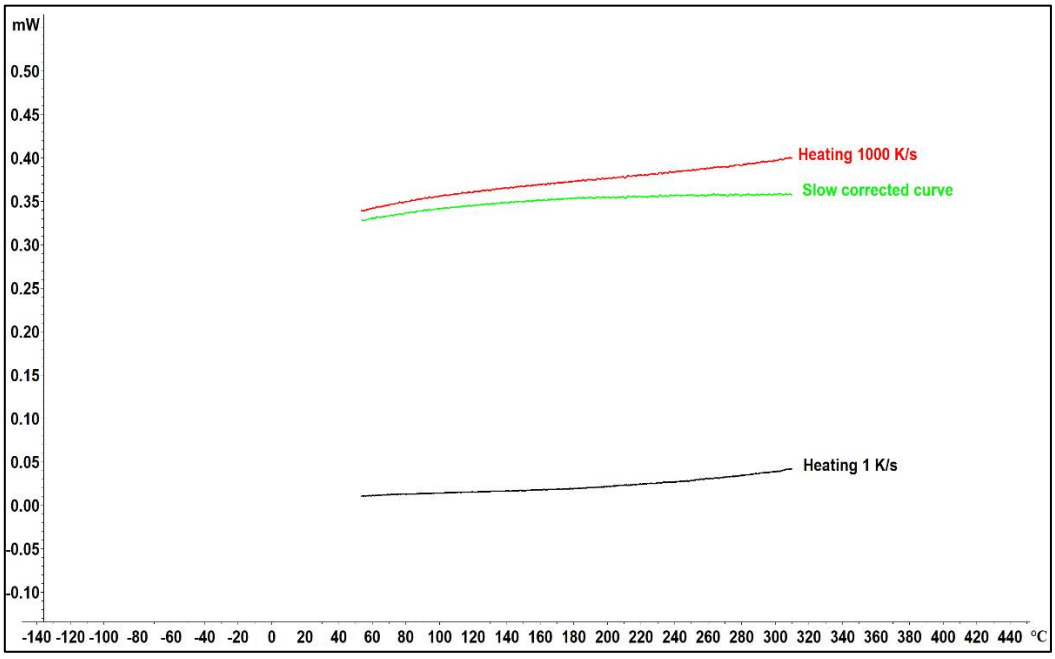

Figure 5-14: *Heat flow corrected curve obtained from the heating of Pb pure sample by slow-rate correction*

Figure 5-15 shows the data obtained by implementing slow-rate correction for the evaluation of the specific heat of a high-purity lead sample. Compared to the results obtained with the symmetry correction and the analyses carried out on the sample of high-purity aluminium, with this second procedure it can be observed a slight overestimation

of the results, compared to the theoretical data. However, it should be noted that the analyses on lead were performed using a different type of sensor, MultiSTAR UFS1, and for this reason comparison between the different experimental curves do not yield any useful conclusions.

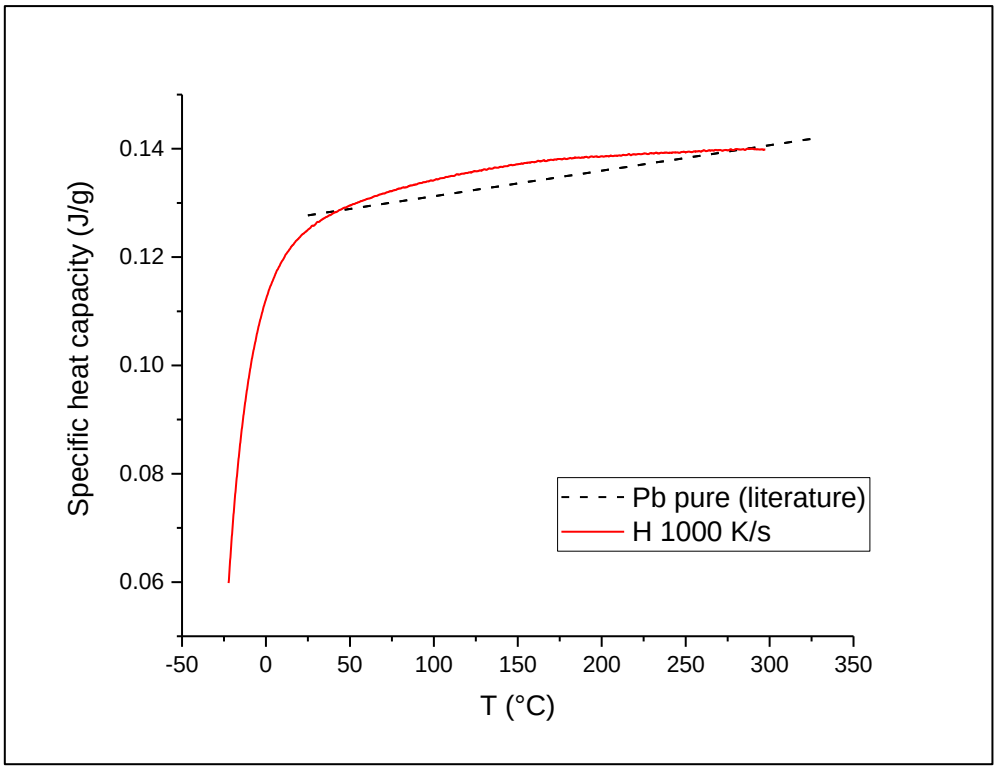

Figure 5-15: *Specific heat capacity trend of high-purity lead, obtained with slow-rate correction (Heating = 1000 K/s)*

In accordance with what was reported in [41], the heat loss function calculated with both methodologies is certainly the same, even if the mathematical procedures of calculation change. The symmetry correction can be considered easier, at least in terms of required analysis time, since it does not involve implementation of low scanning rate measurements. On the other hand, slow-rate correction is much more appropriate when analysing materials in which phase transformations can occur. The AlSi10Mg and the Scalmalloy, being aluminium alloys, if subjected to certain thermal programs, depending on the set temperatures and scanning speeds, can undergo meta-stable phase transformation. However, the use of symmetry correction does not allow the identification of such transformations because of the nature of the correction calculation. In [29] and [30], it has been observed how the occurrence of a given metastable

transformation can be identified thanks to the presence in the heat flow curves of exothermic or endothermic peaks. Since these peaks are present mirroringly both heating and cooling curves, the calculation of the average curve automatically leads to their loss. This problem is not found for slow correction, since the experimental curves, relative to the different rates set, are always subtracted from the curve obtained at 1 K/s.

During this project, therefore, an attempt was made to implement slow-rate correction also for the two aluminium alloys analysed, using MultiSTAR UFH1 sensors, since it was necessary to reach temperatures higher than the melting point of these alloys. However, as shown in Figure 5-16, the curve relative to 1 K/s is higher than the curves obtained for higher speeds, not allowing the effective calculation of the specific heat. It is believed that this problem is exclusively due to the type of sensor used, and in particular to its gradual degradation given the high thermal conditions set.

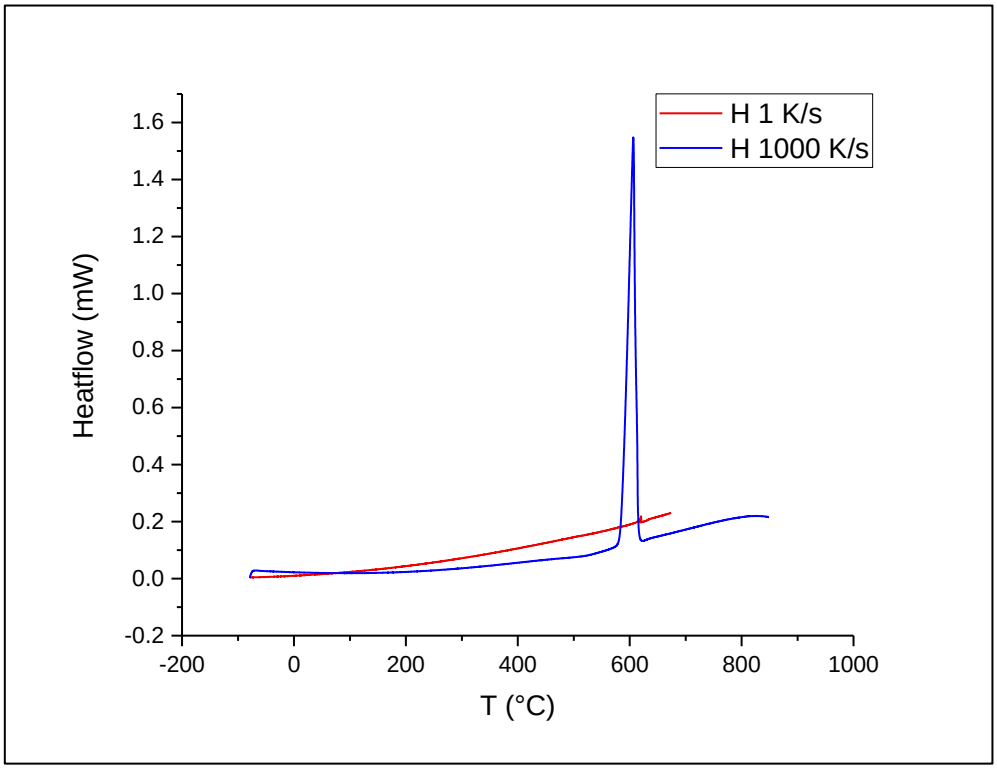

Figure 5-16: *Compare curve at 1 K/s and 1000 K/s*

6. Conclusion

The aim of this thesis project was to exploit the analysis capabilities of the Fast Differential Scanning Calorimetry, in order to evaluate the overall trend of the specific heat of two different aluminium alloys. The use of this characterization technique was essential to emulate the condition imposed in Additive Manufacturing techniques, in which AlSi10Mg and Scalmalloy® are widely used.

From the different results reported in the previous chapters, it can certainly be affirmed that this method of characterization allows obtaining results in accordance with the different theories, especially with regard to the general increasing trend of the specific heat capacity with the temperature. From this point of view, good reproducibility of the real results can be confirmed.

Despite the encouraging reproducibility of the results, in terms of an increasing trend, several inconsistencies with respect to the theoretical data can still be underlined. The causes to which it is thought that these inconsistencies can be traced are of different nature. In general, they may be due either to the sample characteristics, in terms of composition and morphology, or to the method of analysis itself.

As regards the characteristics of the sample, it must initially be considered how the composition of the material is an important variable to be considered, for the evaluation of the specific heat. It has been observed that the presence of specific alloy elements can lead to a drastic variation of this property, compared to the value of the base metal. However, among the different elements found in the global composition of powders, surely what is the main cause of incongruence is oxygen. The presence of oxygen in metal powder, in fact, can lead to the formation of a layer of surface oxide, which affect the achievement of an efficient thermal contact between sensor and sample. Therefore, there is an increase in the phenomenon of thermal lag.

However, the cause of thermal lag cannot be attributed exclusively to the overall composition of the sample but is also related to its morphology. The use of micrometric powders of an approximately spherical shape further reduces the thermal contact compared to the case in which a sample with a much more flattened morphology is used.

The inefficient thermal contact between the sample and the analysis sensor, may also cause inconsistencies in the calculation of the actual mass of the sample. This phenomenon is another possible cause of underestimation of the experimental values of specific heat. An improvement on the mass determination might be achievable by evaluating the mass at a variety of heating rates [41], not just 100 K/s employed in the various experiments.

Significant deviations from the theoretical values can also be caused by the characterization technique, and the analysis procedure implemented. In fact, it was found that the use of a flow of refrigerant argon at 80 ml/min, necessary for cooling the sample, causes an asymmetry between the cooling and heating phases. In particular, the actual cooling rate achieved may be lower than that which is programmed, especially at high scanning rates. This phenomenon represents one of the main causes of underestimation of the experimental data when the symmetrical correction procedure is implemented. A possible solution to this problem could be to modify the type of gas employed, using gas with greater heat conductivity, such as helium or a helium-nitrogen mixture, so as to increase the achievable cooling rate. Also, the gas flow in the analysis chamber could be increased, taking care not to adversely affect the heating phase.

Finally, the correction procedure used is not perfectly appropriate for the analyses performed. In fact, the use of the symmetry correction does not allow observation of any phase transition. For this reason, it would be more appropriate to use the slow-rate correction.

Acknowledgments

During the development of this master thesis project, I was able to expand my knowledge gained in previous years of study. That is why I would like to thank Prof. Stefan Pogatscher for giving me the opportunity to work with his research group at the Montanuniversität Leoben - Chair of Nonferrous Metallurgy. I would also like to thank Cameron Quick for sharing his knowledge about the use of the FDSC technique and for following me throughout my studies in Austria.

I also thank Prof. Irene Calliari for her willingness to play the role of my rapporteur and for allowing me to participate in this 5-month Erasmus project.

I would also like to sincerely thank my wonderful family, from my parents, Chiara and Tobia and my sister Elena, to all my uncles, cousins and grandparents, and especially my grandmother Maria, for supporting me during all my studies and all my experiences. A special thanks is given to my girlfriend Diletta, who I could always rely on to motivate and support me in all my choices.

Finally, a special thank you to all my friends and to all the people with whom I had the good fortune to share all my experiences throughout my university studies.

References

[1] ASTM-International: ‘Standard terminology for additive manufacturing technologies’, vol. F2792-12a, ed. West Conshohocken, PA, ASTM International, 2012.

[2] Li, Y.; Gu, D. Parametric analysis of thermal behavior during selective laser melting additive manufacturing of aluminum alloy powder. Mater. Des. 2014, 63, 856–867.

[3] Kim, D.-K.; Woo, W.; Hwang, J.-H.; An, K.; Choi, S.-H. Stress partitioning behavior of an AlSi10Mg alloy produced by selective laser melting during tensile deformation using in situ neutron diffraction. J. Alloys Compd. 2016, 686, 281–286.

[4] J.H. Martin, B.D. Yahata, J.M. Hundley, J.A. Mayer, T.A. Schaedler, T.M. Pollock, 3D printing of high-strength aluminium alloys, Nature 549 (2017) 365-369.

[5] S. Das, D.L. Bourell, S.S. Babu; Metallic materials for 3D printing; MRS Bull. 41 (2016) 729-740.

[6] N.T. Aboulkhair, N.M. Everitt, I. Maskery, I. Ashcroft, C. Tuck; Selective laser melting of aluminium alloys; MRS Bull. 42 (2017) 311-319.

[7] Tang, M., Pistorius P.C.; Oxides, porosity and fatigue performance of AlSi10Mg parts produced by selective laser melting. Int. J. Fatigue 2016, 94, 192–201.

[8] Olakanmi, E.O.; Cochrane, R.F.; Dalgarno, K.W. A review on selective laser sintering/melting (SLS/SLM) of aluminium alloy powders: Processing, microstructure, and properties. Prog. Mater. Sci

[9] Li, X.P.; Ji, G.; Chen, Z.; Addad, A.; Wu, Y.; Wang, H.W.; Vleugels, J.; van Humbeeck, J.; Kruth, J.P. Selective laser melting of nano-TiB2 decorated AlSi10Mg alloy with high fracture strength and ductility. Acta Mater. 2017, 129, 183–193.

[10] Fousová, M.; Dvorský, D.; Michalcová, A.; Vojt?ech, D. Changes in the microstructure and mechanical properties of additively manufactured AlSi10Mg alloy after exposure to elevated temperatures. Mater Charact. 2018, 137, 119–126

[11] Collins, F. R. & Dudas, J. H. Preventing weld cracks in high-strength aluminium alloys. Weld. J. 45, 241 (1966).

[12] Q. Jia, P. Rometsch, S. Cao, K. Zhang, X. Wu; Toward a high strenght aluminium alloy development methodology for selective laser melting.

[13] B. Ferrar , L. Mullen , E. Jones , R. Stamp , C.J. Sutcliffe; Gas flow effect on selective laser melting (SLM)manufacturing performance; J. Mater. Process. Technol . 212 (2), 355 (2012).

[14] X.J. Wang , L.C. Zhang , M.H. Fang , T.B. Sercombe; The effect of atmosphere on the structure and properties of a selective laser melted Al-12Si alloy; Mater. Sci. Eng. A 597 , 370 (2014).

[15] Rai, R., Elmer, J.W., Palmer, T.A., DebRoy, T., 2007. Heat transfer and fluid flow duringkeyhole mode laser welding of tantalum, Ti-6Al-4V, 304L stainless steel andvanadium. J. Phys. D: Appl. Phys. 40, 5753–5766.

[16] X. Su , Y. Yang; Research on track overlapping during selective laser melting of powders; J. Mater. Process. Technol . 212 (10), 2074 (2012).

[17] N.T. Aboulkhair , N.M. Everitt , I. Ashcroft , C. Tuck; Reducing porosity in AlSi10Mg parts processed by selective laser melting; Addit. Manuf . 1 , 77 (2014).

[18] W.E. King, H.D.Barth, V.M.Castillo, G.F.Gallegos, J.W.Gibbs, D.E.Hahn, C.Kamath, A.M. Rubenchik; Observation of keyhole-mode laser melting in laser powder-bedfusion additive manufacturing (2014)

[19] A.M. Zahra, C.Y. Zahra, G. Jaroma-Weiland, G. Neur, W. Lacom; Heat capacities of aluminium alloys (1995)

[20] Livschitz, B.G.: Physikalische Eigenschaften der Metalle und Legierungen, Leipzig: VEB Deutscher Verlag Grundstoffindustrie, 1989.

[21] T. Hirata j. jap. Inst. Met. Japan, 36 [1972] 1159.

[22] V.s* Keyloviski Metallofizika, Kiev, USSR, 44 [1973] 88.

[23] Denlinger DW, Abarra EN, Allen K, Rooney PW, Messer MT, Watson SK, et al. Thin film microcalorimeter for heat capacity measurements from 1.5 to 800 K. Rev Sci Instrum 1994;65:946–59.

[24] Hager NE. Thin heater calorimeter. Rev Sci Instrum 1964;35:618–24.

[25] Allen LH, Ramanath G, Lai SL, Ma Z, Lee S, Allman DDJ, et al. 1 000 000 °C/s thin film electrical heater: in situ resistivity measurements of Al and Ti/Si thin films during ultra rapid thermal annealing. Appl Phys Lett 1994;64:417–9.

[26] Lai SL, Guo JY, Petrova V, Ramanath G, Allen LH. Size-dependent melting properties of small tin particles: nanocalorimetric measurements. Phys Rev Lett 1996;77:99–102.

[27] Efremov MY, Olson EA, Zhang M, Schiettekatte F, Zhang Z, Allen LH. Ultrasensitive, fast, thin-film differential scanning calorimeter. Rev Sci Instrum 2003;75:179–91.

[28] Lopeandía AF, Cerdó L, Clavaguera-Mora MT, Arana LR, Jensen KF, Muñoz FJ, et al. Sensitive power compensated scanning calorimeter for analysis of phase transformations in small samples. Rev Sci Instrum 2005;76:065104.

[29] Zhuravlev E, Schick C. Fast scanning power compensated differential scanning nano-calorimeter: 1. the device. Thermochim Acta 2010;505:1–13.

[30] Zhuravlev E, Schick C. Fast scanning power compensated differential scanning nano-calorimeter: 2. heat capacity analysis. Thermochim Acta 2010;505:14–21.

[31] S. Pogatscher, D. Leutenegger, J.E.K. Schawe, P. Maris, R. Schaublin, P.J. Uggowitzer, J.F. Loffler; Monotropic polymorphism in a glass-forming metallic alloy. J. Phys.: Condens. Matter 30 (2018)

[32] F. Spieckermann, I. Steffny, X. Bian, S. Ketov, M. Stoica, J. Eckert. Fast and direct determination of fragility in metallic glasses using chip calorimetry. Heliyon 5 (2019)

[33] Y. Corvis, A. Wurm, C. Schick, P. Espeau, Vitreous State Characterization of Pharmaceutical Compounds Degrading upon Melting by Using Fast Scanning Calorimetry, The journal of physical chemistry. B 119 (2015) 6848–6851

[34] L.A. Chapman; Application of high temperature DSC technique to nickel based superalloys; Journal of materials science 39 (2004), 7229-7236

[35] G. Höhne, W. Hemminger, H.-J. Flammersheim, Differential Scanning Calorimetry, 2nd ed., Springer Berlin, Berlin, 2010.

[36] P.J. Haines, Principles of thermal analysis and calorimetry, Royal Society of Chemistry, Cambridge, 2002.

[37] Matthias Wagner, Thermal Analysis in Practice: Collected Applications, 2009.

[38] S. Pogatscher, P.J. Uggowitzer, J.F. Loffler; In-situ probing of metallic glass formation and crystallization upon heating and cooling via fast differential scanning calorimetry

[39] C. Schick, V. Mathot, Fast Scanning Calorimetry, Springer International Publishing; Imprint: Springer, Cham, 2016.

[40] S. Pogatscher, D. Leutenegger, A. Hagmann, P.J. Uggowitzer, J.F. Löffler, Characterization of bulk metallic glasses via fast differential scanning calorimetry, Thermochim. Acta 590 (2014) 84-90.

[41] C.R. Quick, J.E.K. Schawe, P.J. Uggowitzer, S. Pogatscher, Measurements of specific heat capacity via fast scanning calorimetry - accuracy and loss correction, Thermochim. Acta 677 (2019) 12-20.

[42] A. Aversa, G. Marchese, A. Saboori, E. Bassini, D. Manfredi, S. Biamino, D. Ugues, P. Fino, M. Lombardi; New aluminium alloys specifically designed for laser powder bed fusion: a review; Materials (2019)

[43] P. Yang, L.A. Deibler, D.R. Bradley, D.K. Stefan, J.D. Carrol; Microstructure evolution and thermal properties of an additively manufactured, solution treatable AlSi10Mg part

[44] Sercombe, T.B.; Li, X. Selective laser melting of aluminium and aluminium metal matrix composites: Review. Mater. Technol. 2016, 31, 77–85.

[45] T. Herding, O. Kebler, H.W. Zoch, Spray formed and rolled aluminium-magnesiumscandium alloys with high scandium content, Materialwiss. Werkstofftech. 38 (2007) 855-861.

[46] A.B. Spierings, K. Dawson, P. Dumitraschkewitz, S. Pogatscher, K. Wegener, Microstructure characterization of SLM-processed Al-Mg-Sc-Zr alloy in the heat treated and HIPed condition, Addit. Manuf. 20 (2018) 173-181.

[47] Z. Li, B. Li, P. Bai, B. Liu, Y. Wang; Research on the thermal behaviour of a selective laser melted aluminium alloy: simulation and experiment; Materials (2018)

[48] AP WORKS; Material data sheet - Scalmalloy

[49] Metter Toledo; Flash DSC2+: user manual